Optical superoscillation technologies beyond the diffraction limit

Nikolay I. Zheludev [1,2 ✉] *and Guanghui Yuan* [2,3 ✉]

Abstract | Optical superoscillations are rapid, subwavelength spatial variations of the intensity and phase of light, occurring in complex electromagnetic fields formed by the interference of several coherent waves. The discovery of superoscillations stimulated a revision of the limits of classical electromagnetism — in particular, the studies of phenomena such as unlimitedly small energy hotspots, phase singularities, energy backflow, anomalously high wavevectors and their intriguing similarities to the evanescent plasmonic fields on metals. In recent years, the understanding of superoscillatory light has led to the development of superoscillatory lensing, imaging and metrology technologies. Dielectric, metallic and metamaterial nanostructured superoscillatory lenses have been introduced that are able to create hotspots smaller than allowed by conventional lenses. Far-field, label-free, non-intrusive deeply subwavelength super-resolution imaging and metrology techniques that exploit high light localization and rapid variation of phase in superoscillatory fields have also been developed, including new approaches based on artificial intelligence. We review the fundamental properties of superoscillatory optical fields and examine emerging technological applications.

[1]*Optoelectronics Research Centre and Centre for Photonic Metamaterials, University of Southampton, Southampton, UK.*

[2]*Centre for Disruptive Photonic Technologies, The Photonics Institute, School of Physical and Mathematical Sciences, Nanyang Technological University, Singapore, Singapore.*

[3]*Present address: Department of Optics and Optical Engineering, University of Science and Technology of China, Hefei, China.*

✉*e-mail: zheludev@soton.ac.uk; ghyuan@ustc.edu.cn*

Common wisdom in the optics and electromagnetic research communities holds that a 'band-limited' function cannot oscillate faster than the highest Fourier harmonics of its spectrum. This view has serious implications for optics, in particular, for the resolution performance of optical instruments: the spot size of a perfect lens cannot be smaller than half the wavelength of light. This wisdom is also closely related to the Abbe diffraction limit.

Moreover, it is often assumed that light fields in free space cannot change significantly on a scale smaller than half the wavelength. This observation has been used to justify the importance of plasmonics that allows highly confined electromagnetic excitations with large wavevectors at metal surfaces and, therefore, enables the control of light on the subwavelength scale[1,2]. Similarly, the diffraction limit of conventional optics has been the main stimulus of research on metamaterial superlenses, which would allow optical resolution beyond the diffraction limit by conveying the large wavevector evanescent fields from the object to the image[3,4].

However, this wisdom is challenged by the phenomenon of superoscillations, which implies that, for any fixed bandwidth, there could exist finite-energy signals that oscillate arbitrarily fast over arbitrarily long time intervals, and that free space light can have deeply subwavelength structural features. In fact, Maxwell's electrodynamics allows light to be focused to a hotspot of any given size, and the resolution of optical microscopes is not limited to half the wavelength.

In this Review, we explain and illustrate the concept of superoscillations and explore its implications for optics. We discuss the intensity profiles and phase structures of typical scalar and vectorial superoscillatory fields used in optics and overview different technologies for superoscillatory lenses (SOLs). We describe the important technological opportunities provided by superoscillations, including optical super-resolution microscopy with superoscillatory light illumination and sub-diffraction imaging and 'optical ruler' metrology that exploits topological features of the superoscillatory light field. We overview works on THz, acoustic and radio-frequency superoscillations and superoscillations in the wavefunction of an electron and a single photon, and look at the intriguing phenomena of suboscillations and optical energy backflow in complex optical beams.

Functions that oscillate faster than the highest frequency in their Fourier spectrum

As Michael Berry and Sandu Popescu once noticed, functions can locally oscillate faster than their fastest Fourier component of the spectrum, because, in the Wigner representations, the local Fourier transform can have both positive and negative values, which causes subtle cancellations in the Fourier integration over the

Key points

- Light can be focused into a sub-diffraction superoscillatory hotspot of any shape and size beyond the 'diffraction limit' by lenses constructed as a gradient, metamaterial or binary intensity and phase masks.

- Superoscillatory lenses can be used for label-free, far-field, non-invasive imaging with super-resolution that is determined by the size of the superoscillatory hotspot.

- The structure of superoscillatory optical fields has striking similarities with plasmonic fields and contains singularities and deeply subwavelength features of rapid phase variation and energy backflow. These features can be used in nanoscale optical metrology.

- The high sensitivity of scattering of superoscillatory light to the object's shape features can be used for optical imaging with deeply subwavelength, molecular-level resolution, in which reconstructing the object from the scattering pattern is performed by machine learning.

whole function[5,6]. In other words, a function can oscillate fast within a limited segment of its argument in such a way that the Fourier components of the function outside of the segment cancel these high-frequency components. Thus, superoscillatory functions are functions that locally oscillate faster than the highest Fourier component in the spectrum of the entire function.

Careful engineering of functions is required to achieve perfect cancellation. However, many examples of superoscillatory functions have been identified and several techniques have been developed to construct useful superoscillatory functions[5,7–16], including superoscillatory functions with discrete spectrum, such as $f(x) = \sum_{n=0}^{n=5} a_n \cos(2\pi n x)$, where $a_0 = 1$, $a_1 = 13295000$, $a_2 = -30802818$, $a_3 = 26581909$, $a_4 = -10836909$ and $a_5 = 1762818$. Near $x = 0$, this function oscillates several times faster than its highest spectral component at frequency 10π (REF.[17]).

Superoscillatory functions can also have continuous spectra, and such functions are often required for description of practical situations in optics. So-called prolate spheroidal wavefunctions[18] (FIG. 1a) are useful for the decomposition of superoscillatory functions. Prolate spheroidal wavefunctions are band-limited in the finite spectral interval, orthonormal and are exact zeros outside the boundaries of the spectral interval. The pioneering work on prolate spheroidal wavefunctions in applications to signal processing can be dated to the 1960s[19].

FIGURE 1b–e shows an example of a function with continuous spectrum $F(x) = A(x)e^{i\varphi(x)} = 1.8126S_2 + S_3$, which is constructed from just two circular prolate spheroidal functions S_2 and S_3. $F(x)$ exhibits the main characteristic features of superoscillatory functions:

- Band-limited nature. The highest frequency in the spectrum of $F(x)$ is π (FIG. 1e).
- Fast local oscillations. Around $x = 0$, $F(x)$ oscillates more than two times faster than the highest frequency component of its spectrum (FIG. 1c).
- Low amplitude of fast local oscillations. The amplitude of a superoscillatory function is large outside the superoscillating segment (FIG. 1b,c).
- Rapid phase variations. The phase $\varphi(x)$ of the function changes very fast near the low-intensity regions,

where the speed of phase variation exceeds the speed of phase variation of the highest harmonic in the spectrum (FIG. 1d), that is, $|\frac{\partial \varphi(x)}{\partial x}| > \pi$.

- Broad local spectrum. The spectrum of the central part of the function is much broader than the spectrum of the entire function (FIG. 1e). (Such a relationship between the spectrum of the entire function and its segment is a necessary characteristic of superoscillatory functions, but it is not a sufficient one and, therefore, shall not be used as a definition of superoscillatory functions.) Note that the spectrum of the entire function is bandwidth-limited to $\pm\pi$, whereas the central part has a much broader spectrum, explaining the faster oscillation in the interval $[-0.52, 0.52]$.

The properties of superoscillatory functions have been studied intensely[10,20–22]. Properties include an exponential growth of the total energy of a superoscillatory function with the number of superoscillations. At the same time, the energy of a superoscillation (such as a superoscillatory hotspot in optics) reduces only polynomially with its size[20]. This polynomial scaling is important for some super-resolution imaging applications that benefit from the small size of energy hotspots (as discussed in the section on confocal superoscillatory imaging).

From an information theory perspective[20,23], for any fixed bandwidth, finite-energy signals that oscillate arbitrarily fast over arbitrarily long time intervals can exist, but only in signals that possess amplitudes of widely different scales.

The ability of superoscillatory functions to contain rapidly oscillating segments allows encoding of large amounts of information into an arbitrarily short segment of a low-bandwidth signal in such a way that "a symphony of Beethoven can be part of a 1 Hz bandlimited signal"[23]. However, the signal amplitudes in these segments diminish exponentially with the amount of encoded information. Therefore, from the standpoint of information theory, such encoding does not contradict the Shannon theorem[24] that demands exponential increase of the signal power to allow for information compression in a signal with limited bandwidth at a given signal-to-noise level.

Superoscillatory focusing of light

In quantum physics, phenomena relevant to superoscillations have been discussed in the late 1980s by Yakir Aharonov and others. It was noted that weak measurement of a quantum system can result in expectation values much higher than the spectrum of the operator[25,26]. Manifestations of this phenomenon include superluminal velocities in evanescent optical fields[27] and random waves[28], and the apparent displacement of a beam resulting from a slight change of polarization state owing to the spin Hall effect on photons[29].

However, most importantly in optics, the phenomenon of superoscillations offers the opportunity to focus light into a 2D or 3D sub-diffraction hotspot smaller than possible with a conventional lens. The ability to focus light into a hotspot smaller than the diffraction

limit was noted in the 1950s[30] with reference to earlier work on super-gain (super-directive) antennas[31]. Focusing and imaging capabilities based on this work were explored in the early 2000s[32,33], but their relevance to the phenomenon of superoscillations discussed in the context of quantum mechanics[25,26] was not identified at that stage.

A 2006 paper reported the prediction that superoscillations can be realized in classical optics when a periodic diffraction grating produces superoscillations in a propagating beam without evanescent waves[5]. A work linking experimentally observed small light localizations (hotspots) and superoscillations was reported in 2007 (REF.[34]). It demonstrated that the quasi-crystal array of nanoholes in a metal screen can 'focus' light at distances of several tens of wavelengths from the screen, where subwavelength spots are formed without evanescent waves. This work was a peculiar realization of a SOL. The array produces superoscillatory foci of energy concentration in the 'focal plane', harvesting light with a variety of transverse wavevector components emerging from a large number of holes in the array with a continuous spatial spectrum. These hotspots are mapped by scanning across the 'focal plane' with a probe that has a subwavelength optical aperture at its end. Colourful 'photonic carpets' were observed with a conventional optical microscope focused at different heights above the quasiperiodic nanohole array illuminated with a white light[35].

Another step in the experimental study of superoscillations was the realization that superoscillatory hotspots can be directly imaged by a conventional optical microscope with no distortion[35]. Indeed, this imaging is possible because the superoscillatory features are formed by free-space waves away from the diffraction mask and their spatial spectrum contains no evanescent components. Consequently, imaging of these features can be achieved with a conventional optical instrument that has higher numerical aperture (NA_i) than that of the superoscillatory field generator (NA_s). The latter can be evaluated from the size D of the mask generating the superoscillatory hotspot and the distance F at which the hotspot is created as follows $NA_s = \sin\theta = \frac{D}{\sqrt{4F^2 + D^2}}$ (FIG. 2a). This work[35] also anticipated that superoscillations "may provide a new way to achieve subwavelength imaging in the far-field, different from the approaches based on the recovery of evanescent waves".

It was later shown that a subwavelength focus of any size and shape in an area beyond the evanescent fields can be created by diffracting a plane coherent wave on a dedicated mask with continuous variation of optical density and phase retardation[9]. An explicit recipe for the mask design includes the following steps:

- Decide on the desired hotspot size and profile in the focal plane. In principle, any size of the hotspot is possible (bearing in mind that the proportion of energy that can be focused into the hotspot reduces polynomially with the hotspot size)[21].
- Approximate the desired hotspot by a series of prolate spheroidal wavefunctions within a limited interval (this is possible as the functions make an orthonormal set).
- Back-propagate the hotspot field from the focal plane to the plane of the mask (this is possible because the functions of the series are band-limited). The required spatial variation of the field intensity and phase are, thus, known.

A useful superoscillatory hotspot at wavelength λ can be constructed by interference of only two
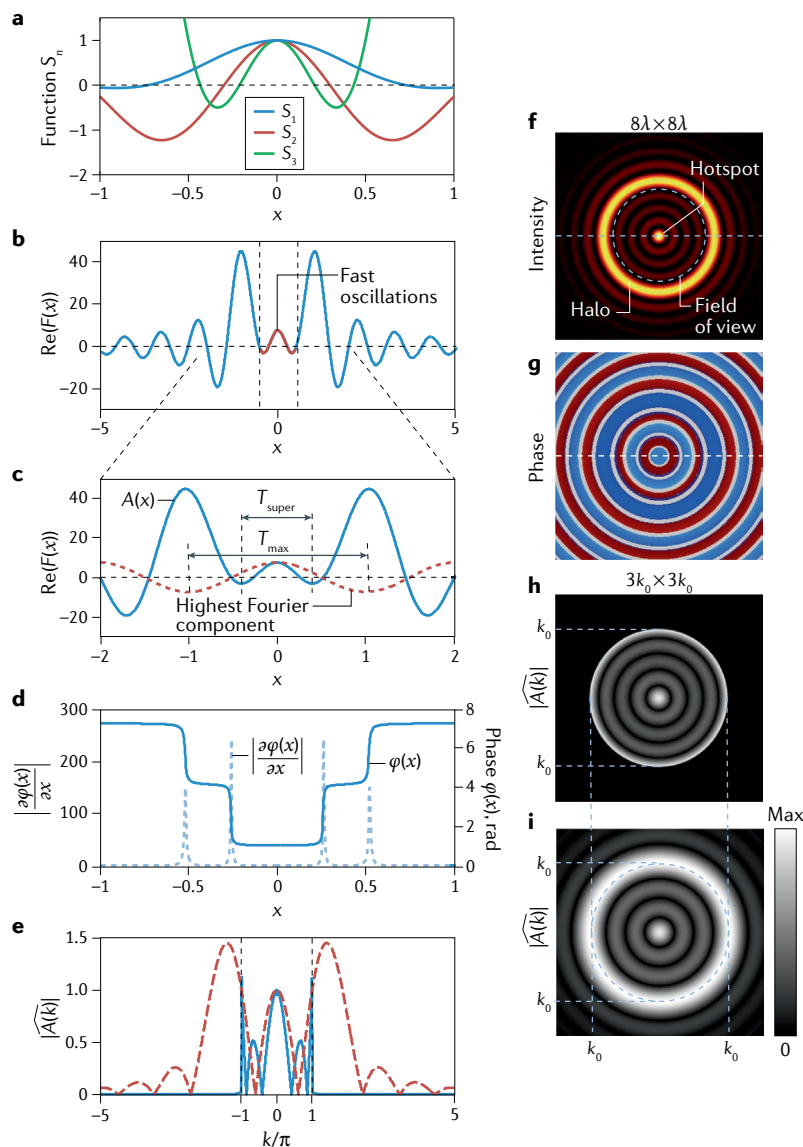
Fig. 1 | **Functions can oscillate faster than their highest Fourier harmonics.**
a | The first three even-order prolate spheroidal wavefunctions S_1, S_2 and S_3. **b–e** | An example of a complex superoscillatory function: function profile (part **b**); zoom-in of its profile $A(x)$ near $x=0$ (blue line) compared with its highest Fourier component (part **c**), where T_{super} and T_{max} denote the spatial extension of the superoscillatory region and period of highest Fourier component, respectively; the phase φ of the function (blue line) and modulus of its gradient (dashed blue line) (part **d**); modulus of the amplitude of the Fourier spectrum $\overline{F(k)} = \overline{A(k)} \times \exp[i\overline{\varphi(k)}]$ of function $F(x)$ (part **e**). $|\widehat{A(k)}|$ is calculated in the x interval $[-\infty, \infty]$ (solid blue line) and in the x interval $[-0.52, 0.52]$ (dashed red line), $x=0.52$ is the zero point of $F(x)$. **f–i** | A 2D superoscillatory focus of coherent light at wavelength λ: intensity map (part **f**); phase map (part **g**); the band-limited spectrum of the entire superoscillatory function (part **h**) and the spectrum of field within the field of view indicated by the dashed light blue circle in part **f** (part **i**).
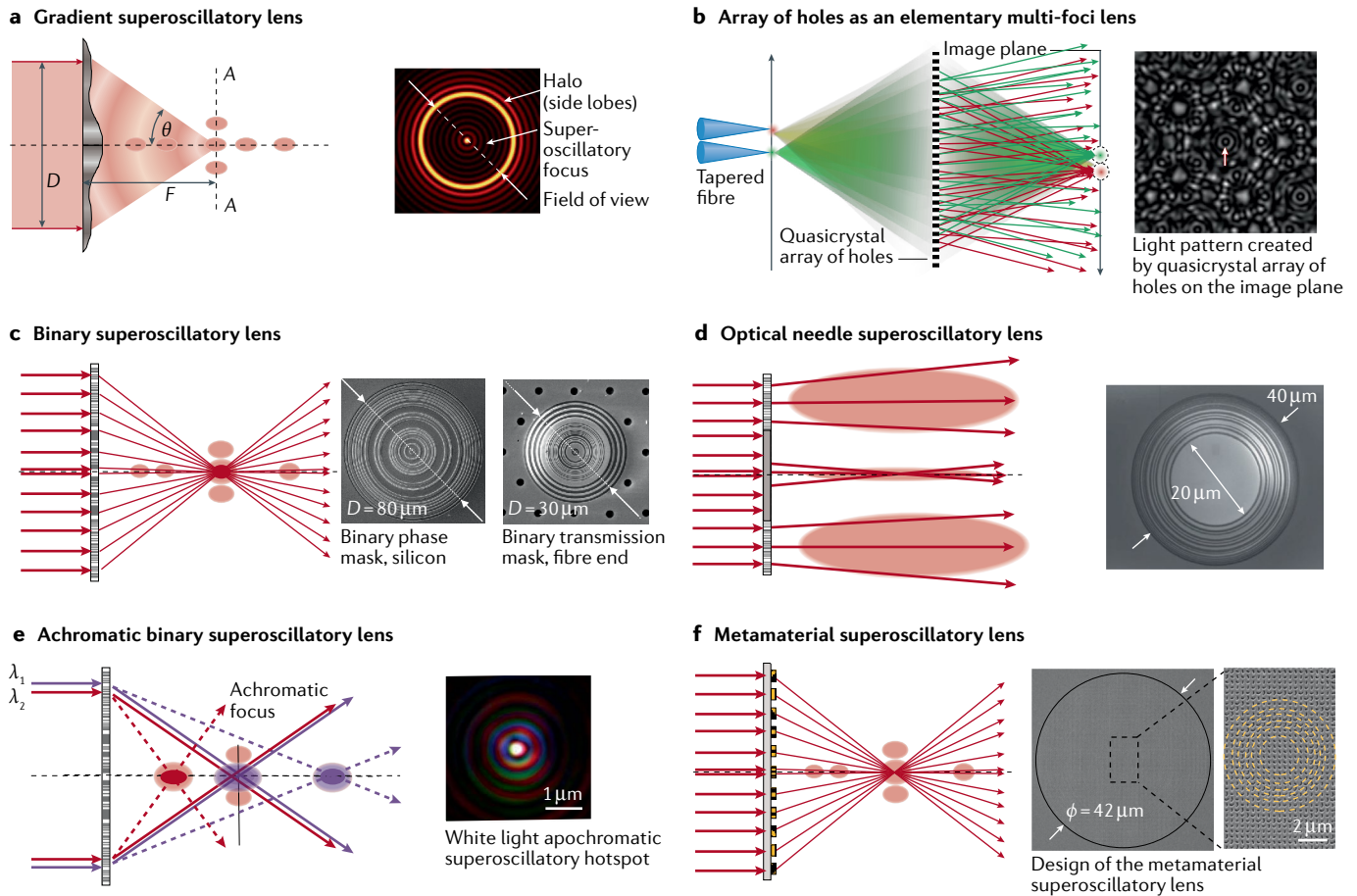
a Gradient superoscillatory lens

Halo (side lobes)
Super-oscillatory focus
Field of view

b Array of holes as an elementary multi-foci lens

Image plane
Tapered fibre
Quasicrystal array of holes

Light pattern created by quasicrystal array of holes on the image plane

c Binary superoscillatory lens

$D = 80\,\mu m$
$D = 30\,\mu m$
Binary phase mask, silicon
Binary transmission mask, fibre end

d Optical needle superoscillatory lens

$40\,\mu m$
$20\,\mu m$

e Achromatic binary superoscillatory lens

λ_1
λ_2

Achromatic focus

$1\,\mu m$
White light apochromatic superoscillatory hotspot

f Metamaterial superoscillatory lens

$\phi = 42\,\mu m$
$2\,\mu m$
Design of the metamaterial superoscillatory lens

Fig. 2 | **Static superoscillatory lenses. a** | Superoscillatory focusing using a mask with precisely engendered continuous variation of transmissivity and phase retardation. **b** | Superoscillatory focusing by a quasicrystal array of nanoholes. **c** | Superoscillatory focusing by a binary mask. **d** | Superoscillatory 'optical needle' focusing. **e** | Achromatic superoscillatory focusing. λ_1 and λ_2 are two wavelengths of light. **f** | Superoscillatory focusing by a metamaterial superlens. θ, half focal angle; A, superoscillatory plane; D, mask size; F, focal distance. Part **b** adapted with permission from REF.[35], IOP Publishing. Part **c** adapted from REF.[60], CC BY 4.0. Part **d** adapted with permission from REF.[71], AIP Publishing. Part **e** adapted from REF.[60], CC BY 4.0. Part **f** adapted with permission from REF.[78], APS.

prolate spheroidal wavefunctions[36] $F(r) = A(r)e^{i\varphi(r)} = 0.2291 \times S_4(r) + S_5(r)$ (FIG. 1f–i). The superoscillatory hotspot (formed with numerical aperture NA = 0.9) is smaller than the focus of a conventional lens, but only a fraction of the energy of the light is concentrated in the superoscillatory hotspot (FIG. 1f). The hotspot is surrounded by concentric zones of rapid phase variation, where the local wavevector $k_{loc} = \frac{\partial \varphi}{\partial r}$ is larger than the amplitude of the wavevector in free space $k_0 = \frac{2\pi}{\lambda}$ (FIG. 1g). The spatial spectrum of the entire hotspot including the 'halo' (the area surrounding the low-intensity zone near the hotspot) is band-limited (FIG. 1h), whereas the hotspot itself has a much broader spectrum (FIG. 1i). On account of the polarization properties of light, the structure of the superoscillatory hotspot becomes more complex than that in the scalar approximation, which is especially noticeable for superoscillatory fields with high numerical aperture (Supplementary Fig. 1). To mitigate the effects of polarization conversion during focusing, in metrology and imaging applications of superoscillatory detectors, polarization filters are often used.

We note that superoscillatory focusing into a hotspot of arbitrarily small size is only possible for the central hotspot. If the full extent of the light intensity distribution at the focal plane is taken into account, the generalized 'common-sense' Abbe criterion still holds for the spot size, into which 50% of the incident power can be focused[37]. Superoscillatory focusing is also compatible with the limitations of the uncertainty principle[38], when the broadened spectrum of the central hotspot is taken into account. However, as discussed below, the band-limited nature of the hotspot and rapid phase variation in its vicinity open opportunities for high-resolution optical metrology and deeply subwavelength imaging.

Technologies of SOLs

Multi-foci SOLs. It became clear in the early stages of research on optical superoscillations that superoscillatory hotspots could be used for imaging. Coherent light diffracted by a quasicrystal array of nanoholes in a metal screen creates a complex volume distribution of hotspots (FIG. 2b). Such an array of holes can act as an

elementary multi-foci lens that images light emanating from the end of a tapered fibre to a screen at the image plane: upon moving the fibre end, the superoscillatory hotspot moves in the opposite direction on the imaging plane, as appropriate for a convex lens, and creates a real inverted image of the object[39]. However, although multiple foci in the imaging plane are advantageous for some imaging modalities[40], most applications require lenses with a single hotspot.

Continuous profile SOLs. A mask with precisely engineered continuous variation of transmissivity and retardation can create a superoscillatory focus of any size or shape[9]. For photonics applications, masks with radial symmetry are often used. Typically, the small hotspot created by the mask at the focal plane is surrounded by a 'halo'. The diameter of the superoscillatory 'field of view' (the low-intensity area between that hotspot and the halo) is important: larger fields of view simplify applications, but reduce the fraction of incident light's power focused into the central hotspot. Manufacturing a mask with precise gradients of transmissivity and retardation is a formidable challenge. An advanced photolithography method has been demonstrated to create a greyscale density SOL. The technique uses femtosecond laser pulses to induce phase-change transitions in a thin layer of material that locally controls the exposure dose to photoresist, thus, enabling a 3D sculpting with greyscale density variation and submicron lateral resolution[41]. However, SOLs with simultaneous continuous greyscale variation of optical density (transmission) and optical thickness (retardation) have not yet been demonstrated.

Binary SOLs. Currently, most SOLs are constructed with binary intensity or phase masks. A binary mask is a pattern in which either optical density or phase retardation can take two fixed values: transparent–opaque in the case of intensity masks or a 180° phase difference for the phase masks. No exact universal analytical expressions are known for reverse designing of binary masks unless certain approximations are made[42]. Instead, the particle swarm optimization technique has been widely employed[43–48]. Typically, the merit functions for optimization include the size of the central spot, numerical aperture and size of the usable field of view. A similar approach is used to design binary phase masks. Evolutionary[49] and genetic algorithms[50–53], optimization-free methods[54,55] and artificial intelligence algorithms are also being used for superoscillatory binary lens design.

By construction, the binary masks resemble Fresnel zone plates but are more complex. Binary intensity masks are either concentric arrays of holes[56,57] or a 'matryoshka' arrangement of concentrically enclosed slits in an opaque screen, typically a metal film[43,46,58,59] (FIG. 2c). Binary SOLs are fabricated using standard nanofabrication approaches: focused ion beam (FIB) milling, electron beam lithography, photolithography and etching. FIB is the simplest way to fabricate binary-amplitude SOLs. After depositing a thin layer of metal films on a transparent substrate, the film is

directly milled to remove those parts of the mask that are to transmit light. In general, harder metals, such as chromium or titanium, take longer to mill in the FIB, but give better fabrication quality. Binary intensity SOLs have been demonstrated at flat substrates, at ends of large mode diameter photonic crystal fibres[60], at gradient-index lenses and by structuring atomic thin layers of chalcogenide semiconductors[61]. The step-type phase masks have been fabricated in silicon and silica by optical lithography[62,63], and rewritable and reconfigurable SOLs have been demonstrated using phase-change materials[64].

The most technologically advanced binary phase SOLs were fabricated in a high-throughput optical lithography process on a large silica wafer[62]. They were optimized for the wavelength of 633 nm, having diameter of $2R = 1.22$ mm and focal distance of $F = 200$ μm. A conventional lens with such parameters has $NA = R/\sqrt{F^2 + R^2} = 0.95$ and focuses into a hotspot of $\delta = \lambda/(2NA) = 335$ nm, or $\delta = 0.53\lambda$. The SOL focuses light into the hotspot of $\delta_{SOL} = 253$ nm, or $\delta_{SOL} = 0.4\lambda$. The effective numerical aperture of the SOL is $NA_{eff} = \lambda/(2\delta_{SOL}) = 1.25$. Such a numerical aperture can only be achieved with SOLs. It is not possible to reach $NA \geq 1$ with a conventional lens or gradient metasurface lens[65,66] focusing in free space. Conventional high-numerical-aperture lenses are often complex and usually very expensive (thousands of dollars), whereas quartz phase SOLs are flat, simple in construction and cheap in production. Quartz phase SOLs have negligible absorption loss and can sustain high light intensities.

Immersion, in particular, solid immersion (that is, placing a layer of high-refractive-index dielectric between the lens and the focal plane), reduces the size of the superoscillatory hotspot even further[67,68]. Obvious shortfalls of the SOLs are the presence of a halo and low throughput efficiency into the hotspot that limits some applications, such as light-assisted manufacturing.

'Optical needle' SOLs. Often, the design of a SOL is optimized to achieve a small hotspot at a particular distance from the mask. The depth of focus (DOF) of a conventional lens[69] is linked to its numerical aperture $DOF \sim \lambda/NA^2$. For high-numerical-aperture lenses, the hotspot is smaller and $DOF \sim \lambda$. However, many applications, including data storage, metrology and manufacturing with light, benefit from long DOF.

Channelling light into a radiation 'needle stick' was discussed with reference to Albert Einstein's "Einsteinschen Nadelstichstralung" in the early 1920s[70]. Remarkably, binary SOLs can be engineered to produce such a 'needle stick' — a hotspot with very long depth of focus along the axial direction in such a way that, at any cross section, the hotspot remains smaller than the 'diffraction limit' allows. Such light patterns are termed optical needles[71–75] (FIG. 2d). Optimization of optical needles can involve blocking the central part of the lens, thus, preventing nearly coaxial diffracted waves reaching the focus. For example, a sub-diffraction binary intensity, circularly polarized optical needle generator with a transverse spot size of 0.45λ and axial depth of focus

of 15λ has been demonstrated at a violet wavelength of 405 nm (REF.[73]).

Potential applications for optical needle lenses include high-density optical storage and heat-assisted magnetic recording, a technology that aims to increase the density of magnetic recording. Existing heat-assisted magnetic recording schemes depend on a light-induced local heating of the magnetic information carrier to enable the magnetic switching that records data. Near-field plasmonic transducers have been proposed as light concentrators[76], but superoscillatory lenses provide an alternative. A superoscillatory solid immersion lens with $NA_{eff} = 4.17$ has been demonstrated that can focus light from a laser source operating at 473 nm into sub-50-nm hotspots on the magnetic recording layer[77]. Similarly, a SOL may be used for readout of optical memory with pitch between data marks less than $\lambda/4$, thus, enabling higher density data storage than conventional lenses offer[56].

Achromatic SOLs. SOLs typically create a chain of foci along the lens axis. The position of foci on the axial line depends on the wavelength of light, and multiple foci at different wavelengths can overlap. Achromatic SOLs have been engineered in such a way that one of these foci on a particular wavelength overlaps with another focus at a different wavelength (FIG. 2e). Simultaneous apochromatic focusing of three different wavelengths (red, green, blue) has also been demonstrated[60]. Apochromatic sub-diffraction SOLs could serve as super-resolved focusing and imaging tools for applications in metrology, low-cost microscopy, high-resolution quantum correlation measurements, pump–probe experiments for ultra-fast dynamics, excitation and collection of photoluminescence, coherent anti-Stokes Raman scattering for super-resolution and non-linear imaging, and nanofabrication using two-photon or three-photon absorption.

Metamaterial SOLs. The well-known metamaterial superlens uses a slab of negative index metamaterial to recover evanescent waves from the object in the image plane. This powerful idea is not yet implemented as a practical imaging device and its realization in the optical part of the spectrum faces a number of challenges. However, the metamaterial approach is a practical way of creating a different type of superlens that does not use evanescent waves but, instead, creates superoscillatory foci in the far field from the lens. We call it the superoscillatory metamaterial lens (FIG. 2f).

The nearly complete design freedom on transmissivity and retardation of the lens mask can be achieved using a metasurface. In such a lens, light is scattered on a planar array of 'metamolecules' — individual scatterers that provide the prescribed levels of phase delay and scattering amplitude at different radial positions on the lens — in such a way that the entire array diffracts light into a superoscillatory hotspot. A plasmonic metamaterial SOL can reach sub-diffraction hotspots on fields of view up to 6λ in diameter and robustly perform in imaging applications[78]. A metamaterial SOL with effective numerical aperture $NA_{eff} = 1.52$ and focus as

small as 0.33λ in size has been demonstrated. It contains 8,500 metamolecules forming a lens of 40 μm in diameter.

To design such a lens, first, a planar continuous gradient amplitude and phase mask necessary to transform an incident plane wave into a superoscillatory hotspot is calculated, as described above. Second, a library is defined of subwavelength plasmonic metamolecules with individual scattering characteristics mimicking and matching the amplitude and phase characteristics found anywhere on the continuous mask. Each metamolecule is a V-shaped nanoslit cut into a thin gold film, a design that can be easily adjusted to control the polarization state, intensity and phase of the scattered wave by adjusting length, opening angle of the V shape and width of the slits[79,80]. Third, the mask is simplified as a concentric array of metamolecules, to provide the same attenuation and retardation as the continuous mask in the points of their locations.

Superoscillatory metamaterial lenses achieve smaller hotspots with better throughput efficiency than binary masks. They can be manufactured by well-established nanomanufacturing techniques and are scalable to operate at any wavelength. Broadband superoscillatory metasurfaces based on geometrical phase modulations have also been demonstrated[81,82]. The simplest form of a binary metamaterial SOL is a cylindrical SOL, a 1D metamaterial pattern[83].

Single-photon regime of SOLs. Applications of SOLs in quantum super-resolution imaging, quantum lithography and biomedical imaging often require low light intensity. The question, therefore, emerges whether superoscillatory focusing is possible in a single-photon regime. This question is, in fact, relevant to the cornerstone question of wave–particle duality of photons: does the Young's double slit diffraction experiment work in a single-photon regime, one photon at a time[84]? Studies of SOL performance in a single-photon regime have been undertaken with a cylindrical metasurface SOL[83]. The superoscillatory hotspot observed in the single-photon regime by detecting a pattern created by a large number of individual photons at the focal plane was the same as that created with coherent laser illumination. This experiment provided direct evidence that the wavefunction of a single photon can superoscillate and contain sub-diffraction features with length scale smaller than that constructed with allowable wavevector eigenvalues, thus, linking the classical[26] and quantum[25] manifestations of the phenomenon of superoscillations.

Although binary masks provide a robust and simple way to implement subwavelength hotspot generators, they generate static superoscillatory fields. Superoscillatory focusing could also be achieved by using spatial light modulators (SLMs) to create a beam with carefully designed amplitude and phase profile for tailored interference.

Double SLM superoscillatory generator. Precise programmable shaping of the beam may be achieved with a pair of analogue liquid crystal SLMs, one of

which controls the phase profile of the beam and the other controls its intensity profile. The modulated beam is then imaged onto the back focal plane of the microscope objective. In this way, any arbitrary field profile may be obtained at the microscope focal plane simply by encoding its Fourier spectra on the SLMs. For a review of the technology, see REFS[85,86], and for details on its implementation, see REF.[87]. The double SLM technology is robust and, apart from imaging applications (see below), it is used for atom trapping in cold atom experiments (Supplementary Fig. 2a,b). Superoscillatory focusing has also been used in other high-resolution optical trapping and manipulation applications[88,89], in which the trapping potential provides unprecedented localization accuracy and stiffness, significantly exceeding those of conventional diffraction-limited beams.

Digital micromirror superoscillatory light generator. Full control of the phase and intensity can also be achieved with a single binary SLM based on the digital micromirror device (DMD; Supplementary Fig. 2c). A DMD chip is a micro-opto-electromechanical system that has millions of microscopic mirrors on its surface arranged in a rectangular pixelated array. Such chips are widely used in digital image projectors. The mirrors, typically 16 μm across, can be individually switched on torsion hinges by electrostatic force between two orientations corresponding to on or off states (Supplementary Fig. 2c). Beams with arbitrary phase and intensity profiles are generated using a method termed 'digital holographic grating'[90,91], in which a computer-generated hologram, which carries the amplitude and phase information of the desired light beam, is designed and loaded as a binary mask on a DMD. The first-order diffraction on this holographic grating is the target light beam, which is designed as a superoscillatory hotspot.

SOL versus SLM. SLM superoscillatory focusing has a number of experimental differences to focusing with binary static SOLs. The SLM approach allows focal spots to be formed at the focus of a microscope objective, giving a working distance of a few hundred microns, compared with the few tens of microns typically achieved with static binary SOLs. SLM superoscillatory focusing can also be combined with active scanning of the hotspot across the object by controlling the beam direction with SLMs. SLMs also enable creation of 'volume superoscillation', in which a 3D focal spot beyond the 'diffraction limit' can be achieved using a superposition of shifted Bessel beams with different longitudinal wavevectors and orbital angular momenta[92]. However, the SLM system is more complex to align, consisting of a number of optical components, and is considerably larger than static SOLs, which have only one component that is relatively easy to align with the input laser beam.

THz, acoustic and radio-frequency superoscillations. The concept of superoscillatory focusing is complementary to the concepts of super-directive microwave antennas of limited size that can direct radiation into an arbitrarily narrow beam by precisely tailoring the interference of waves emitted by different elements of the array[31,93,94]. It has been explored in the microwave part of the spectrum but was abandoned because of low throughput efficiency of such antennas. However, the studies and development of applications of superoscillations in focusing is now extended to the THz electromagnetic frequency range[49,95,96]. A superoscillatory metalens at 0.327 THz with a resolution below the diffraction limit has been demonstrated[49]. A THz far-field sub-diffraction optical needle for a wavelength of 118.8 μm with focal length 420λ and radius 160λ has been demonstrated for applications in super-resolution THz tomography[95]. An ultrasonic binary SOL has been developed for super-resolution ultrasound imaging and tweezing application[97,98]. Superoscillatory focusing and radar imaging have also been observed in the radio-frequency regime[99,100].

Superoscillations in complex fields

Although dedicated superoscillatory field generators and SOLs can create prescribed hotspots, superoscillations also commonly appear in complex light fields[101,102]. Importantly, a wide range of complex electromagnetic field structures created by interference of multiple coherent light waves can have deeply subwavelength features in their structures.

Following REF.[103], this can be illustrated by example of a light field $U(r) = U_0(r)e^{i\varphi(r)}e^{i\omega t}$ created by interference of 50 coherent plane waves oscillating at frequency ω, with randomly chosen amplitudes and phases, and propagating in the plane with prevailing direction of propagation along $k_{\parallel}$: $U(r) = \sum_{i=1}^{i=50} A_i e^{i\omega t - k_i r}$, $k_{\parallel} \gg k_{\perp}$. FIGURE 3a shows a fragment of this field pattern that is $4\lambda \times 4\lambda$ in size, in terms of phase.

The map of intensity of the light field (FIG. 3b) features a few energy localization hotspots. Some of them are smaller than allowed by the 'diffraction limit'. For instance, one is only 0.31λ in the transverse direction. Although the overall energy flow is from left to right, the light field also contains zones of energy backflow. In these zones, the predominant direction of the Poynting vector of light is opposite to the predominant direction of the beam propagation, a feature that can often be seen in complex superoscillatory fields. Note that energy backflow zones are often much smaller that the wavelength of light. It has also been noticed that the perimeter of the energy backflow zone contains the phase singularity point and the tangent to the perimeter at this point is directed parallel or antiparallel to the prevailing direction of energy flow[103]. Optical backflow in the direction transverse to the prevailing direction has also been experimentally observed[104].

FIGURE 3c shows a map of intensity $U_0(r)$ overlapped with maps of the zones where the phase of the field changes rapidly perpendicular to the prevailing direction of propagation, along $k_{\perp}$, that is, where $|\nabla\varphi(r)_{\perp}| > |k|$. Narrow areas of these zones (waists) coincide with positions of singularities. The value of $|\nabla\varphi(r)_{\perp}|$ reaches local maxima at the narrow waists, around the singularity points. These zones are deeply subwavelength in
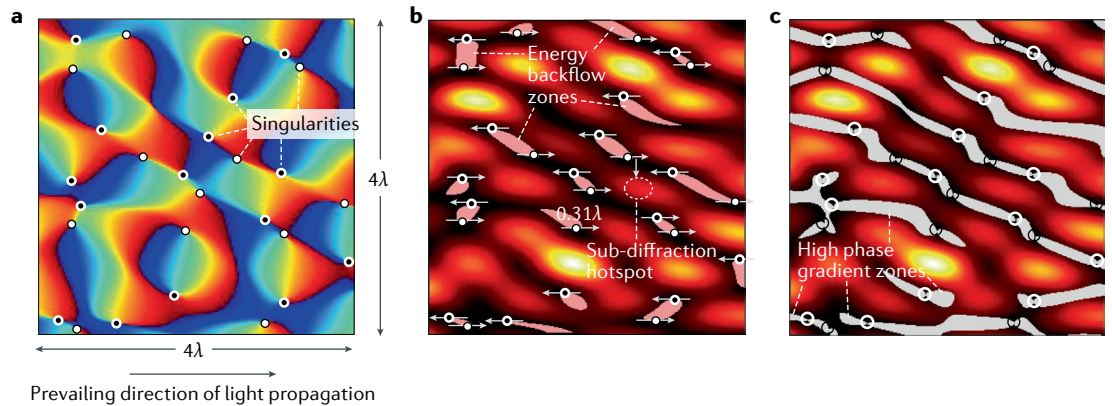
Fig. 3 | **Subwavelength features in complex light fields created by interference of 50 coherent scalar plane waves.**
a | Map of the phase $\varphi(\boldsymbol{r})$ of the resulting electromagnetic field, from $\varphi = -\pi$ (blue) to $\varphi = +\pi$ (red). Circles indicate singularities, points where intensity goes to zero and the phase of the wave is not defined. If by circling around the singularity clockwise the phase increases, a white circle with black core is used; if it results in the phase decrease, a black circle with white core is used. The field of view is $4\lambda \times 4\lambda$, where λ is the wavelength of light. **b** | Intensity of the resulting electromagnetic field, with white corresponding to highest intensity and black corresponding to zero intensity. **c** | The intensity map overlapped with the maps of zones (grey) where the phase of the field changes rapidly perpendicular to the prevailing direction of propagation.

size and the maxima of $|\nabla\varphi(\boldsymbol{r})_\perp|$ are highly localized at singularities.

We discuss below how these subwavelength features of complex coherent electromagnetic fields can be used in super-resolution metrology and imaging, but before that, we describe how these features can be mapped experimentally.

Mapping superoscillatory fields

Experimental evidence of large local wavevectors and energy backflows in superoscillatory optical fields — some of their main features — has only been reported in recent years[105]. Compared with demonstrating intensity hotspots, observing these features in optics is more complex. Such observation relies on being able to measure the phase of the field, to obtain the local wavevectors $\boldsymbol{k}_{\text{local}} = \nabla\varphi$. Because the phase information can only be obtained in interferometric measurements and the fields have fast phase variations, the interferometer must be extremely stable. Spatial resolution far better than a half-wavelength is also required, owing to the small size of investigated features. To meet these challenges, a monolithic metasurface interferometry technique has been developed[105] (Supplementary Fig. 3). In this technique, the superoscillatory field interferes with a reference wave created by the same metamaterial mask, thus, minimizing the instabilities that are characteristic of bulk free-space interferometers.

The field maps in the vicinity of a superoscillatory hotspot reveal four main features of superoscillatory fields (FIG. 4b):

- Sub-diffraction limit hotspots (FIG. 4b and Supplementary Fig. 3c). On the intensity map ($\sim |E_y|^2$), the hotspot size in the x section is smaller than allowed by the Abbe–Rayleigh limit. The focus is surrounded by intense fringes.
- Phase singularities (FIG. 4b and Supplementary Fig. 3d). At the low-intensity regions near the focus,

the hotspots are flanked by phase singularities with topological charges of ±1.
- Giant local wavevectors (FIG. 4b and Supplementary Fig. 3e). The magnitude of the local wavevectors $|k_x|$ near the phase singularities is more than an order of magnitude higher than $k_0 = 2\pi/\lambda$.
- Energy backflow (FIG. 4b and Supplementary Fig. 3f). The energy backflow zones can be derived from the mapping of longitudinal wavevector k_z and are pinned to phase singularities[103]. Maps of the time-averaged Poynting vector $S = \frac{1}{2}\text{Re}\{E \times H^*\}$ (where E is the electric field and H is the magnetic field) show that, in these regions, the incident energy flow is 'trapped' and circulates without propagating in the forward direction (FIG. 4b insets).

These maps illustrate that superoscillatory fields can have subwavelength structural elements. Indeed, in this case, the backflow areas are only about $\lambda/20$ in size along the x direction and areas where $|k_x| > k_0 = \omega/c$ are even smaller, on the order of $\lambda/100$, in line with the predictions reported in REF.[103].

'Plasmonics' in free space

The mapping of superoscillatory fields has revealed some remarkable similarities between the near-field plasmonic focusing by nanostructures and superoscillatory focusing in free space (FIG. 4). Indeed, rapid spatial phase variation, giant local wavevectors and phase singularities are routinely observed in computational experiments on plasmonic nanostructures. In fact, the access to high-value wavevectors is what makes plasmonics a preferred platform for nanophotonic devices. However, a plasmonic field does not propagate into free space; it is a collective excitation of electromagnetic fields and electrons in the evanescent area at the dielectric–metal interface.

Similarities between the superoscillatory and plasmonic fields are striking[105]. For instance, FIG. 4a shows

a silver nanoparticle at plasmonic resonance[106]. One can see energy backflow zones pinned to singularities that resemble the structure of fields at the superoscillatory focus described above. In both plasmonic and superoscillatory foci, zones of energy backflow facilitate the subwavelength localization of light by removing electromagnetic energy from the areas neighbouring the foci, thereby, squeezing the foci.

Moreover, in both plasmonic and superoscillatory focusing, the energy throughput efficiencies scale polynomially with size of the focal spot. Indeed, a deeply subwavelength hole of diameter σ in an opaque screen can be used as a nanoscale light source, for instance, in scanning near-field optical microscopy. Only a small proportion of light illuminating the screen passes through the hole, with throughput efficiency
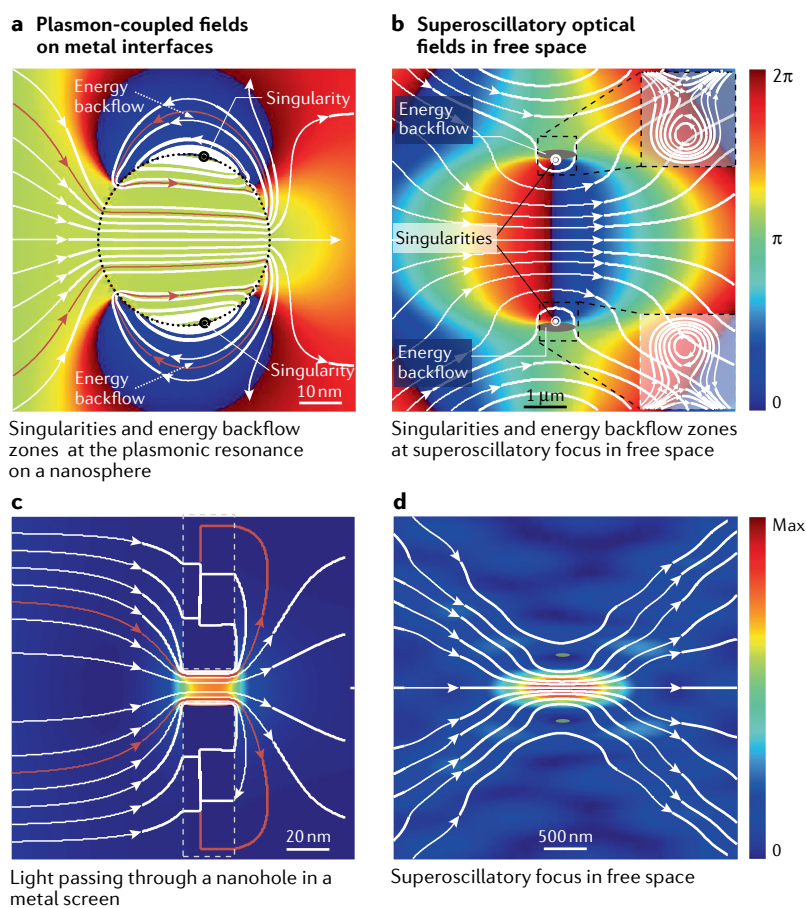
scaling as $(\sigma/\lambda)^4 + O((\sigma/\lambda)^5)$. A small absorbing dielectric or plasmonic nanoparticle of diameter σ also 'focuses' light by harvesting energy of the illuminating plane wave (FIG. 4a) with scattering cross section that scales as $(\sigma/\lambda)^4$. Similarly, in free space, the proportion of energy channelled into a superoscillatory region decreases polynomially with size of the superoscillation[20,56].

Metrology with superoscillations

Light is a useful tool for metrology, as it allows non-disruptive measurements of the size or position of the object against marks of a ruler. Displacement of the object can be measured optically with the help of a conventional lens or microscope, in which case, the resolution is limited by diffraction to about half of the optical wavelength, typically, a fraction of micrometre. Resolution three orders of magnitude better than the diffraction limit can be achieved by using — instead of the physical ruler — an 'optical ruler', using phase singularities of a structured electromagnetic field as marks[107]. Optical ruler metrology exploits the fact that free-space optical fields can be imaged by a conventional lens with no limit to resolution and that the phase information can be retrieved by the monolithic metamaterial interferometry (Supplementary Fig. 3). The optical ruler can be used for measuring the mutual displacement of two platforms, one containing a laser source and a metamaterial mask generating an optical ruler and the other containing a magnifying lens, a polarizer and an image sensor (FIG. 5a).

1D and 2D displacement measurements are possible with the optical ruler. For 1D metrology, the optical ruler light field can be created by a Pancharatnam–Berry phase metasurface, which is constructed as rows of slits oriented at +45° and −45° to the incident polarization. For 2D metrology, the Pancharatnam–Berry phase metasurface can be an array of slits with randomized orientation that creates a superoscillatory speckle optical field. The field created by such metasurfaces is highly structured for the polarization perpendicular to the polarization of the incident light, whereas the light transmitted with incident polarization remains a plane wave. By detecting the intensity of the interference pattern of these waves through a magnifying lens and a polarizer for different polarizations of the incident wave, the phase and intensity profile — and, thus, marks of the optical ruler — can be retrieved with resolution better than $\lambda/800$ (REF.[107]) (FIG. 5b–g).

Optical ruler metrology is a far-field non-contact technique. It has higher resolving power than that of most optical super-resolution and interferometric techniques. Unlike conventional metrological interferometric instruments, it practically does not suffer from mechanical and thermal instabilities. The metasurface can be manufactured at the tip of an optical fibre, allowing numerous applications in which high resolution, small size and non-contact operations are essential, including monitoring displacements of scanning stages, lithography mask alignment, nano-assembly tools and for monitoring the deformation, fatigue or thermal expansion of components.

a Plasmon-coupled fields on metal interfaces

Singularities and energy backflow zones at the plasmonic resonance on a nanosphere

b Superoscillatory optical fields in free space

Singularities and energy backflow zones at superoscillatory focus in free space

c Light passing through a nanohole in a metal screen

d Superoscillatory focus in free space

Fig. 4 | **Similarities between plasmonic fields at metal interfaces and superoscillatory field in free space. a,b** | Compare the phase maps (colour-coded) and the Poynting vector trajectories (solid lines) of a plane wave propagating from left to right and focused by a silver nanosphere of subwavelength diameter at plasmonic resonance[106] (part **a**) and of a free-space field at the superoscillatory hotspot created by diffraction of a plane wave on a 1D metamaterial phase array (part **b**). In both cases, the area of energy concentration is surrounded by singularities (circles) and zones of energy backflow 'squeezing' the flow of energy into the focus. **c,d** | Compare the intensity maps (colour-coded) and the Poynting vector trajectories (solid lines) of a light wave passing through a subwavelength hole in a thin plasmonic gold film indicated by the dashed lines[137] (part **c**) and of the free-space field at the superoscillatory hotspot (part **d**). In both cases, only a fraction of the energy can be channelled into the 'sub-diffraction' hotspot, which is a polynomial function $P(\sigma/\lambda)$ of the ratio between the hotspot diameter σ and the wavelength of light λ. Parts **a** and **b** adapted from REF.[105], CC BY 4.0.
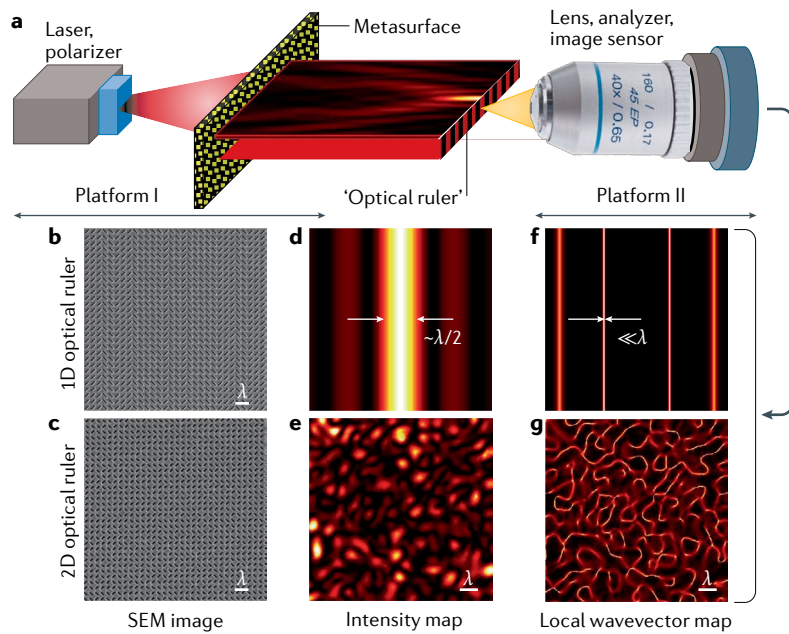
Fig. 5 | **'Optical ruler' metrology. a** | Optical ruler metrology measures the mutual displacements of two platforms, I and II. **b–g** | Optical ruler metrology retrieves intensity maps (parts **d** and **e**) and phase gradient maps (parts **f** and **g**) of the field created by 1D or 2D metasurfaces (parts **b** and **c**) in free space, and uses the zones of strong phase gradient in the superoscillatory field as reference marks of the optical ruler. These zones (lines on maps **f** and **g**) are localized orders of magnitude stronger than the intensity hotspot (maps **d** and **e**), offering nanometric resolution metrology. SEM, scanning electron microscopy; λ, wavelength of light. Adapted with permission from REF.[107], AAAS.

Shortly after REF.[107] was published, we received an interesting comment from M. V. Berry, who put light on the earlier history of using singularities in metrology, in this case, with radio waves[108] (M. V. Berry, personal communication): "We discussed a possible application [of singularities]: measuring movement of polar ice sheets. The idea was to choose a place on the ice surface where the disorderly echo from the bottom displayed a phase singularity, wait overnight while the ice sheet moves, and then explore the surroundings to find a place where the echo was the same as yesterday. With radio waves of length 5 m, the extreme phase sensitivity would enable displacements of a few cm to be detected."

Challenges of imaging

The Abbe–Rayleigh diffraction limit of conventional optical instruments has long been a barrier to studies of microscale and nanoscale objects. Early approaches to overcome the limit were based on recording the shape of the object by registering its optical near field formed by rapidly oscillating but non-propagating waves with large wavevectors: contact photography and scanning near-field optical microscopy.

In contact lithography, the near field is registered by the photographic emulsion placed in contact with the object. The emulsion is detached from the object after exposure to light, leaving its photo-imprint in the emulsion. Unfortunately, contact photography offers no magnification to the level of detail that can be seen by the

naked eye. It is not suitable for super-resolution imaging. However, its modern version, optical mask lithography with short-wavelength light sources, is widely used for semiconductor chip manufacturing.

In scanning near-field optical microscopy, a small aperture or scattering probe captures an object's evanescent field, converts it into propagating waves and directs it to a photodetector. The technique can achieve subwavelength spatial resolution but requires the probe to be scanned in nanoscale proximity of the object. Its applications are limited, as it cannot be used to image inside living cells or semiconductor chips, for example, and image acquisition takes a long time.

A number of metamaterial-based techniques have been proposed to reconstruct and capture evanescent fields, most notably, the far-field Veselago–Pendry 'superlens'. In the superlens, a slab of negative index metamaterial is used to image the evanescent waves from an object onto the imaging plane. This approach, however, faces substantial fundamental and technological challenges in its implementation in optics and has not yet been developed as a practical imaging technique.

Could deeply subwavelength imaging resolution be achieved without detecting the near field? A classical approach for imaging uses a conventional lens that focuses light scattered by the object into the imaging plane with magnification. This approach does not have any limits in magnification, at least in principle, but has a sharp limit on resolution of about half the wavelength.

Nevertheless, far-field super-resolution imaging is possible and, in biological studies, is dominated by stimulated emission depletion (STED) and single-molecule localization microscopies[109,110], which require intense laser illumination and for samples to be labelled with luminescence agents (such as semiconductor quantum dots). These labels are known to change the behaviour of the biological systems; furthermore, labelling cannot be applied to solid artificial nanostructures (such as silicon chips), making these techniques unsuitable for nanotechnology use. The other major far-field super-resolution technique is structured illumination microscopy, in which an object is illuminated with periodically modulated light patterns. However, this approach requires complex post-processing and typically only doubles the resolution of a conventional microscope, unless near-field illumination is used.

Below, we review two approaches to far-field, label-free, super-resolution imaging techniques that use superoscillatory optical fields for sample illumination: confocal superoscillatory imaging and deeply subwavelength topological microscopy.

Confocal superoscillatory imaging. One route to far-field subwavelength imaging is to use an optical superoscillatory hotspot to illuminate the object[43]. The size of the hotspot determines the resolution of confocal microscopy, and the accrued images are themselves superoscillatory and, hence, can reveal fine structural details of the object that are lost in conventional far-field imaging.

This microscopy is a non-algorithmic, low-phototoxicity imaging technology and is a tool for both nanotechnology and biological research of samples that do not allow labelling.

In principle, superoscillatory lenses can be used to image objects that are smaller than the field of view[43,111], but this has not yet been demonstrated experimentally and would have limited practicality. To enable useful applications, the conventional microscope objective lens cannot simply be replaced with a SOL, because, for objects bigger than the field of view, light scattering from the parts of the objects illuminated by the halo distorts the images. This distortion can be mitigated in a confocal microscope if the objective lens is a conventional lens with high numerical aperture, while the sample is illuminated by a SOL with tight focus. Imaging is achieved by scanning the sample relative to the focus of the SOL and using a detector with a small confocal aperture that rejects most of the scattering from the halo-illuminated parts of the image.

The microscope's response is characterized by its point spread function $P_{MIC} = P_{SOL} \times P_{COL}$, where P_{SOL} is the point spread function of the illuminating SOL and P_{COL} is the point spread function of the conventional objective lens. The response is band-limited to spatial frequency $\Phi = 2\pi \times \overline{NA}/\lambda$, where $\overline{NA}$ is the average of the numerical apertures of the illuminating SOL and the imaging lens[87]. If the object has subwavelength structures and the function $O(\boldsymbol{r})$ describing it is not band-limited to Φ, a conventional microscope cannot resolve its fine details beyond $\lambda/(2NA)$. However, the image $I(\boldsymbol{r}) = P_{MIC} \otimes O(\boldsymbol{r})$ created by the superoscillatory microscope is different ($\otimes$ denotes a convolution): it is a superoscillatory function and can, therefore, locally oscillate much faster than Φ and can contain detail finer than $\lambda/(2NA)$. A mathematical example of forming a superoscillatory image in such a band-limited system is presented in REF.[87]. Therefore, the main principle of this microscopy is that superoscillatory illumination of the object creates its superoscillatory image that is band-limited and, thus, can be transferred by free-space waves through a band-limited optical system.

A superoscillatory microscope can be constructed by adding a laser-based superoscillatory illumination system to a conventional confocal microscope. Such a microscope has been demonstrated[43] using a binary transmission mask as a superoscillatory illuminating lens and a laser operating at 640 nm. It resolved nanoscale slits in an opaque screen spaced by a distance of 137 nm and round holes spaced by a distance of 105 nm (0.16λ). The holes were completely unresolved if conventional illumination was used in the same microscope (FIG. 6a). In another example, superoscillatory images of nanostructures taken with a binary superoscillatory optical needle generator are presented in FIG. 6b.

Metamaterial superoscillatory superlenses have also been used in imaging applications[78]. The smaller the sub-diffraction hotspot, the better the resolution of the superoscillatory microscope. With a superoscillatory hotspot of 264 nm (0.33λ), pairs of 160-nm holes in a metal film separated by 120 nm (0.15λ, edge to edge) were resolved with superoscillatory illumination, using a laser source operating at 800 nm. Dielectric binary superoscillatory superlenses manufactured from quartz using complementary metal–oxide–semiconductor-compatible lithography has also been reported[62]. With a laser source at wavelength 633 nm, patterns and pairs of holes spaced by a distance of 110 nm (0.17λ, edge to edge) were resolved with superoscillatory illumination. The conventional bright-field imaging modality was not able to resolve these patterns.

A sophisticated microscopy using SLM-synthetized superoscillatory illumination has been demonstrated[87,112], with high-frame-rate polarization-contrast imaging of unmodified living cells, at a resolution substantially exceeding that achievable with conventional instruments. Superoscillatory illumination was achieved with SLMs (FIG. 6c). The bio-version of a confocal superoscillatory microscope also incorporated a liquid crystal polarization controller to implement an advanced form of polarization contrast imaging, giving high contrast even in unstained transparent biological samples (FIG. 6d). Such non-algorithmic, low-phototoxicity imaging technology is a powerful tool for biological research. Structured illumination microscopy with superoscillatory multi-lobe beams shows similar potentials[113]. Another example of a SLM-based superoscillatory imaging system with far-field working and observation distances[114] is presented in FIG. 6e.

It is educational to compare superoscillatory confocal microscopy with STED microscopy. In STED, fluorescence is depleted in specific regions of the sample, while a central focal spot is left active to emit fluorescence. In contrast, superoscillatory confocal microscopy functions by illuminating the sample locally with a SOL. Both are far-field super-resolution techniques, but STED requires that the sample be labelled with a fluorescent reporter, whereas superoscillatory microscopy works with unlabelled samples. Superoscillatory confocal microscopy is a linear imaging technique working at low light intensities, whereas STED is a non-linear optical technique that requires intense laser radiation to deplete the fluorescence around the central focal spot.

Deeply subwavelength topological microscopy. The far-field confocal superoscillatory imaging described above has a variety of applications, and, in particular, it offers video-frame-rate high-resolution microscopy for demanding bioimaging tasks[87]. However, because the intensity of the superoscillatory hotspot rapidly drops with the hotspot size (while the interference from the halo increases), the signal-to-noise ratio reduces for smaller hotspots needed for higher levels of resolution. In a conventional confocal microscopy setting, it is difficult in practice to reach resolution beyond $\lambda/5$ using superoscillatory illumination. However, two ideas have been explored to make deep subwavelength resolution possible.

The first idea comes from the observation that, in the confocal imaging mode, light scattered on the sample is detected through an aperture and the rest of the

scattered field is blocked. Could the rejected light be useful to construct a better resolved image of the sample? Indeed, different iterative feedback algorithms have been developed to reconstruct an image from the intensity of the scattering patterns of optical, deep ultraviolet and X-ray radiation (scatterometry). In these approaches,
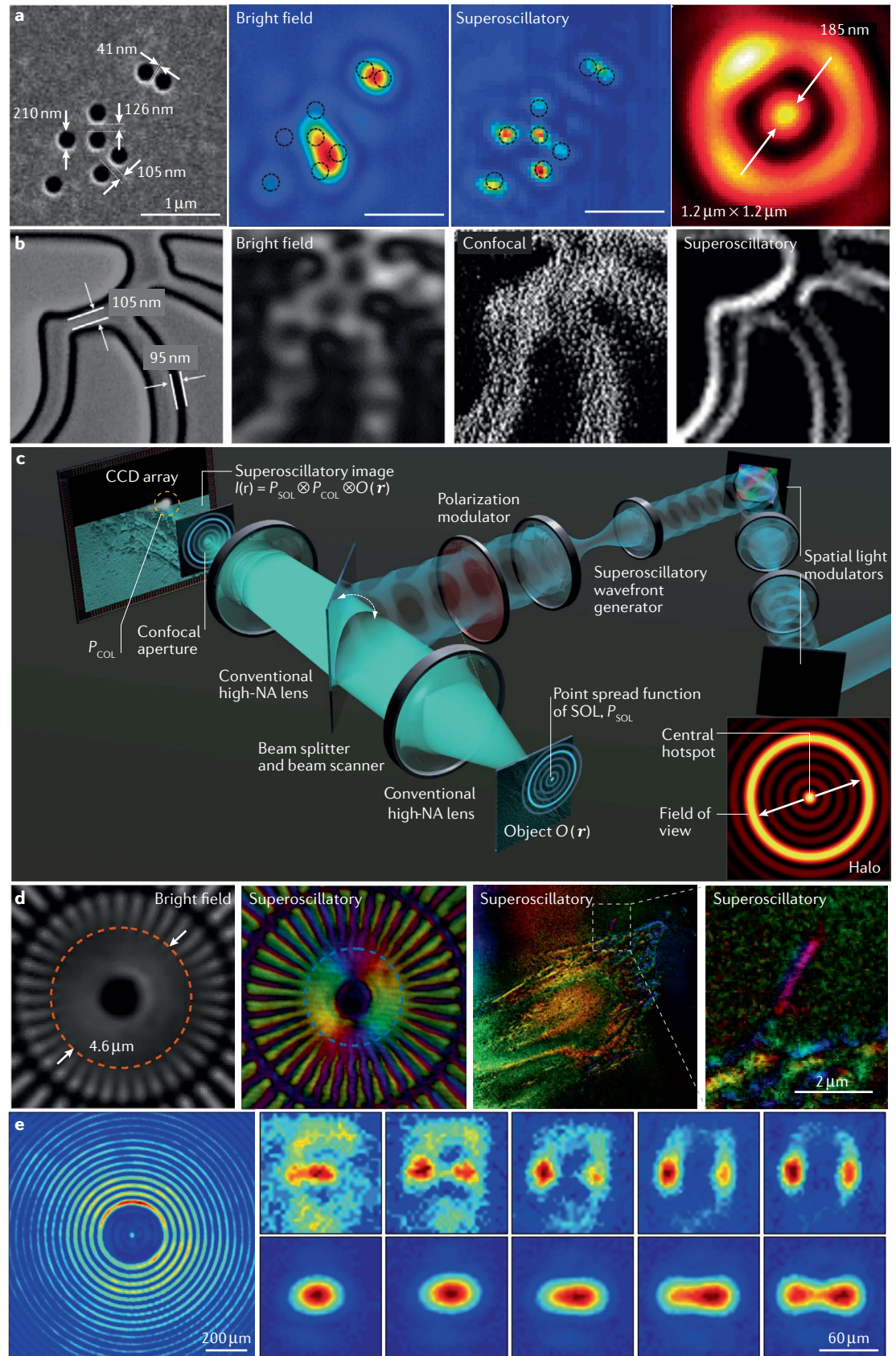
the resolution is limited by the wavelength of the illuminating light in most cases[115], but when compressed sensing techniques for imaging sparse objects are used, the resolution increases fivefold[116].

Thus, the first idea is to use deep learning to solve the inverse scattering problem of imaging. It has been proven mathematically[117] that neural networks are efficient in solving this sort of problem, and deep learning methodology is now widely applied to imaging[118–121]. Indeed, an artificial-intelligence-enabled microscopy has been introduced, which reveals dimensions of an object by analysing its far-field scattering pattern. The object is reconstructed from the intensity profiles of scattered light, while the reconstruction is performed by a neural network trained on a large number of scattering events with similar objects of different sizes. This technique is termed deeply subwavelength optical imaging and has been demonstrated experimentally by imaging dimers with subwavelength features with resolution exceeding $\lambda/20$ (REF.[122]). This technique has also been applied to imaging subwavelength slits in an opaque screen with a resolution of $\lambda/260$ (a few nanometres), thus, challenging the resolution of scanning electron microscopy and FIB milling[123]. Moreover, the counting of subwavelength particles from their diffraction pattern has been demonstrated[124].

This brings us to the second idea. Could deeply subwavelength features of superoscillatory fields — such as zones of rapid variations of phase and energy backflow zones — be exploited for high-resolution microscopy? In essence, can one use topological features of light, such as singularities, to reach and exceed the nanometre-level resolution achieved in 'optical ruler' metrology?

Indeed, the scattered field pattern is sensitive to the placement in the topologically structured field of an absorbing nanoparticle with size of only $\lambda/1,000$ (REFS[107,125]) (FIG. 7b,c) — compared with plane wave illumination, scattering of the superoscillatory field is two to three orders more sensitive to the presence and position of the nanoparticle[105]. This sensitivity is attributed to the presence of steep gradients in the intensity and phase in the superoscillatory field. Indeed, placing or displacing an object in the narrow subwavelength singularity zone results in a strong change of intensity across the detector plane.

These two ideas are combined in deeply subwavelength topological microscopy (DSTM)[125] (FIG. 7). It reveals the fine structure of an object through its far-field scattering pattern when the object is illuminated with light containing deeply subwavelength singularity features. The object is reconstructed from such a pattern by a neural network that is trained on a large number of scattering events on known objects. Numerical experiments on imaging of a dimer have demonstrated resolving powers better than $\lambda/200$ — two orders of magnitude beyond the conventional 'diffraction limit' of $\lambda/2$. Proof-of-principle experimental confirmation of DSTM with a training set of small size, yet, sufficient to achieve resolution fivefold better than the diffraction limit, has also been reported[125].

There are several factors contributing to high-resolution of DSTM:
- From the prospective of Fourier optics, topologically structured superoscillatory illumination gives access to large local wavevectors and ensures that the scattering pattern of structured light is more sensitive to the small features of the imaged object than that of unstructured light.
- From the prospective of information theory, multiple scattering patterns recorded during the training process provide more information for the image retrieval process than what is available in a lens-generated single image.
- For simple objects such as a dimer, the object's sparsity and the existence of prior knowledge about it helps the retrieval process, similarly to how sparsity helps 'blind' compressed sensing techniques.
- The retrieval of the image from its diffraction pattern can be mathematically reduced to solving the Fredholm integral equation. It has been proven mathematically[117] that neural networks are efficient in solving these sorts of problems. Indeed, a deep learning process trained on a large dataset creates a powerful and accurate deconvolution mechanism without using explicit information on the phase of the detected signals. Experiments show that larger training sets give higher resolution.

An interesting direction for future research could be the analysis of resolution limits of microscopies using prior knowledge of the sample and deep learning techniques that give access to the large amount of information accrued during the neural network training process, while the resolution of conventional microscopies is determined by the noise of the system and the size of the imaging aperture[126].

Although, so far, DSTM has been demonstrated for 1D imaging, both computationally and in a

◀ Fig. 6 | **Superoscillatory imaging. a** | Experimental demonstration of a superoscillatory microscope for subwavelength imaging with a resolution up to $\lambda/6$ at $\lambda = 640\,\text{nm}$: object (arrays of nanoholes in metal screen); bright-field image; superoscillatory image; the illumination hotspot created by the binary superoscillatory lens. **b** | Scanning electron microscopy, bright-field, confocal and superoscillatory images of a nanostructure, at wavelength 405 nm. The superoscillatory image is taken with a binary superoscillatory optical needle generator. **c** | Schematic of the confocal biomicroscope with superoscillatory illumination (following REF.[87]). The superoscillatory light field is formed by two spatial light modulators and is focused on the object by a conventional lens creating a sub-diffraction illumination hotspot (inset). A moving semi-transparent mirror is used to scan the hotspot across the sample. The light reflected from the object is detected through a confocal aperture to suppress the effect of a halo surrounding the hotspot. The image is itself a superoscillatory function constructed point by point with resolution determined by the size of the hotspot. **d** | Images taken with the microscope from part **c**: conventional bright-field and superoscillatory images of the 36-sector binary Siemens star test object with resolution limits indicated by dashed red and blue lines. Smaller features of the test object are closer to the centre. A high-frame-rate live image taken of an unlabelled human bone cell, with zoom-ins detailing a single filopodium (an actin-filled protrusion that guides cell migration). **e** | Imaging with a spatial light modulator-based superoscillatory imaging system: point spread function of the microscope, and comparison of the resolving capability of closely spaced apertures: top sub-row, superoscillatory images; bottom sub-row, diffraction-limited images. NA, numerical aperture; P_{COL}, point spread function of the conventional objective lens; P_{SOL}, point spread function of the superoscillatory lens. Part **a** adapted from REF.[43], Springer Nature Limited. Part **b** adapted with permission from REF.[46], Wiley. Part **d** adapted from REF.[87], CC BY 4.0. Part **e** adapted from REF.[114], Springer Nature Limited.

proof-of-principle experiment, it can be readily extended to 2D and 3D objects, as well as objects of random shape. It will be particularly efficient in microscopy of a priori known shapes, such as those found in routine tasks of bioimaging and machine vision. Furthermore, the technique does not require labelling of the sample with luminescent materials, nor intense laser illumination, and is resilient to noise[125].

Beyond optical imaging and metrology

The study of superoscillations is a growing direction of research[127–129]. Apart from imaging and metrology, another emerging direction of superoscillatory technologies is the synthesis of short optical pulses. The shortest optical pulses corresponding to a given optical bandwidth are known as bandwidth-limited pulses or Fourier-transform-limited pulses, or, more commonly, transform-limited pulses. Bandwidth-limited pulses have a constant phase across all frequencies that make up the pulse, and such pulses can be generated by mode-locked lasers. For different pulse shapes, the minimum duration–bandwidth product is different, with the Gaussian pulses having a value of 0.441.

Constructing a light wave from a number of synchronized frequency components can create a superoscillatory periodic pulsation in the time domain that contains bursts of energy that are shorter than the Fourier transform limit for isolated light pulses. This has been demonstrated experimentally by using a grating-based optical pulse shaper to synthesize four optical frequencies in the red part of the spectrum around the wavelength of 801 nm at frequencies 370.9, 373.2, 375.6 and 377.9 THz with carefully adjusted relative amplitudes of 13, 9, 9 and 13 and mode-locked phase of 0, π, π, 0 (REF.[130]) (FIG. 8a). Doing so creates a superoscillatory envelope with a short temporal feature that breaks the temporal Fourier transform limit for isolated light pulse (FIG. 8b). In the experiment, a temporal feature that is approximately three times narrower than a Fourier-limited Gaussian pulse with the same bandwidth was achieved with a visibility around 30%. Such pulses have been used to demonstrate super-resolution in the time domain: two consecutive pulses can be distinguished by mixing them in a non-linear optical process with the superoscillatory signal, whereas mixing the pulses with a transform-limited Gaussian pulse of the same bandwidth fails to resolve them. The improvement of temporal resolution with superoscillatory pulses was also studied in the context of pulse compression using Schelkunoff's superdirective antenna design[131]. Remarkably, time domain superoscillatory optical pulses can be used to transmit high-frequency signals through absorbing media[132] or low-pass filters[133]. A super-narrow frequency conversion using non-linear materials with complex, superoscillatory domain structuring has been demonstrated[134].

Whereas superoscillating functions can locally oscillate faster than their highest Fourier harmonic, suboscillatory functions exist that oscillate slower than their slowest Fourier harmonic[135]. For instance, if a function $f(x) = (\cos x + 2i \sin x)^{10}$ is superoscillatory (FIG. 8c), a function $g(x) = (\cos x + 0.5i \sin x)^{-10}$ is suboscillatory (FIG. 8d). This function has a lower frequency bound of $k_{min} = 10$. Near $x = 0$, it oscillates at a rate of 0.5 times slower than the slowest component of the spectrum, $\cos(10x)$. Whereas superoscillation can lead to superfocusing of light, suboscillations lead to super defocusing of light. Moreover, suboscillatory beams pass around obstacles without reducing the beam spread in the far field, which may be useful in dark-field microscopy.

Superoscillation is a general wave phenomenon and can be observed not only with light and acoustic beams but also with electron de Broglie waves, promising interesting applications in high-resolution electron microscopy. Indeed, superoscillatory focusing of electron waves into a central spot that is smaller than the Abbe–Rayleigh diffraction limit was demonstrated in
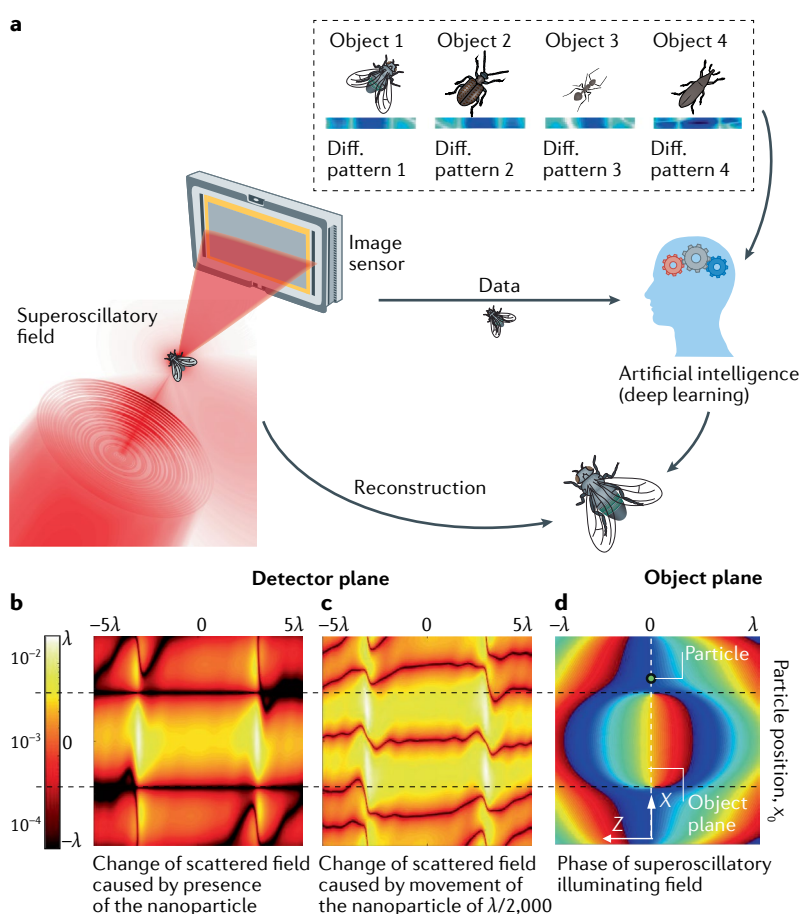
Fig. 7 | **Deeply subwavelength topological microscopy with a superoscillatory light field. a** | The image intensity sensor detects the intensity profile of the diffraction pattern resulting from scattering of the superoscillatory light field on the object. A number of different diffraction patterns are recorded when the illuminating field is scanned against the object. The artificial intelligence programme, trained on a large number of scattering events from known objects, reconstructs the imaged object from the collected data with high resolution. **b–d** | Far-field intensity patterns are sensitive to the presence and position of small absorbing nanoparticles in the image plane of size $\lambda/1{,}000$, where λ is the wavelength of light. The position of the singularity is indicated by the dotted lines. Part **b** shows normalized change of the scattered field intensity profile caused by the presence of the nanoparticle. Part **c** shows normalized change of the scattered field intensity profile caused by shift of the nanoparticle of $\lambda/2{,}000$ along the x direction. Part **d** shows phase profiles of the illuminating superoscillatory field, where light propagates along the positive z axis. Parts **b–d** adapted from REF.[125], CC BY 4.0.
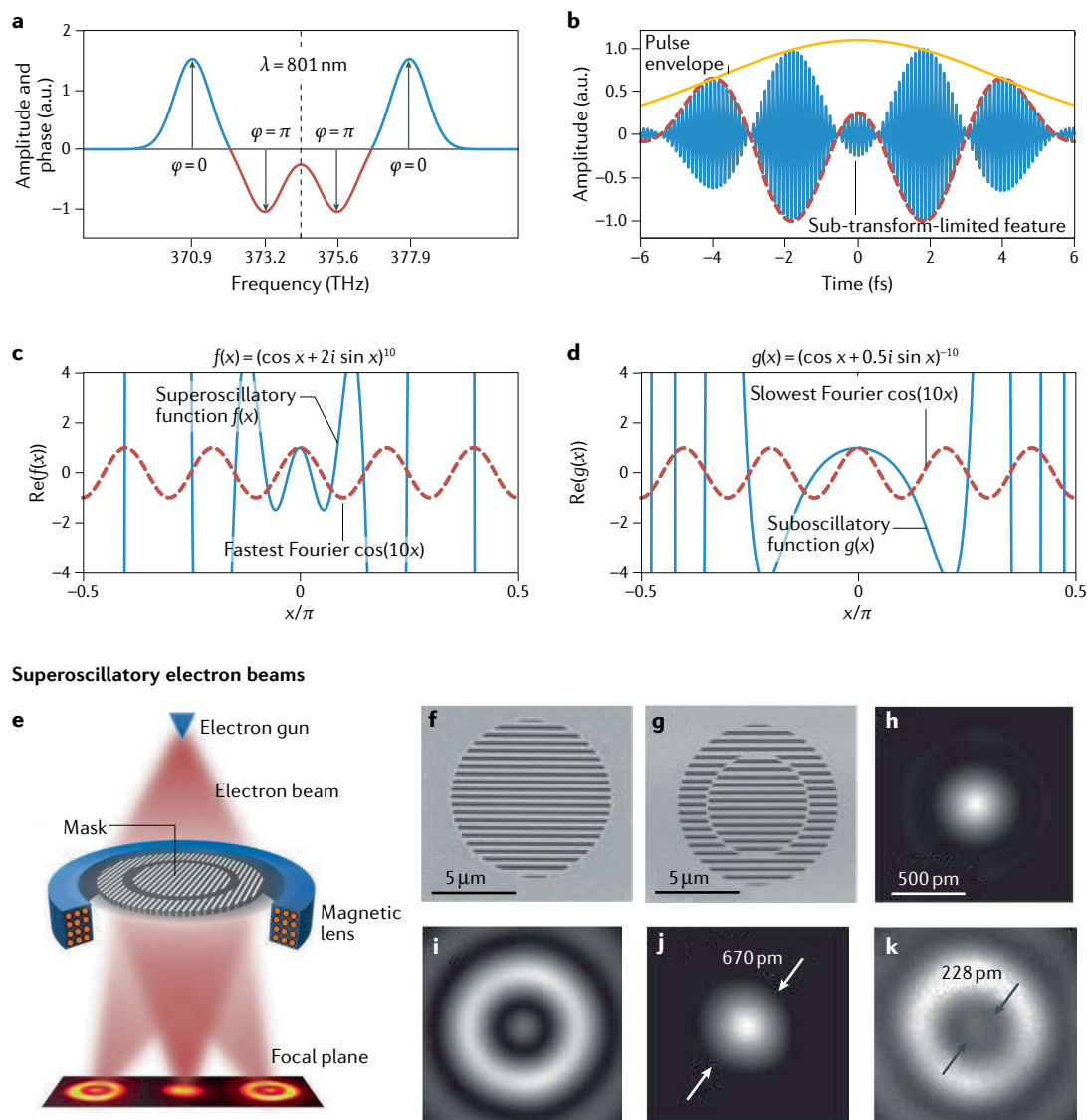
Fig. 8 | **Superoscillations beyond optical imaging and metrology. a,b** | Temporal superoscillations. The spectrum, with locations where the phase φ is 0 or π marked (part **a**), and temporal waveform (part **b**) of a superoscillatory optical beat signal with central wavelength $\lambda = 801$ nm. **c** | A superoscillatory function $f(x)$ (blue solid line) that oscillates faster than its highest spectral Fourier component (red dashed line) near $x = 0$. **d** | A suboscillatory function $g(x)$ (blue solid line) that oscillates slower than its slowest spectral Fourier component (red dashed line) near $x = 0$. **e–k** | An electron microscope (part **e**) with binary diffraction masks (part **f**) or superoscillatory diffraction mask (part **g**) inserted into the electron beam. The desired wavefunction is created in the ±1 diffraction orders. Calculated electron hotspots (parts **h** and **i**) and measured electron hotspots (parts **j** and **k**) obtained experimentally with masks in parts **f** and **g**. The central hotspot in part **k** is much smaller than allowed by the Abbe–Rayleigh diffraction limit in part **j**. Parts **a** and **b** adapted with permission from REF.[130], APS. Parts **c** and **d** adapted with permission from REF.[135], OSA. Parts **e–k** adapted with permission from REF.[136], APS.

a scanning electron microscope[136] (FIG. 8e). A two-zone, off-axis, computer-generated holographic phase mask was used to generate three diffraction orders with the desired superoscillating electron wavefunction at the +1 and −1 diffraction orders. A central superoscillatory hotspot with diameter of 228 pm is experimentally measured, which is 66% smaller than the diffraction-limited Airy spot of 670 pm for the given small numerical aperture of the microscope focusing magnetic lens (the electron's de Broglie wavelength is 2 pm at 300 keV). The degradation of image contrast in the experiment is

mainly attributed to the spatial incoherence of the electron source and inelastic scattering in the supporting substrate of the mask. Here, the electron microscope operates essentially in the single-particle regime, supporting the assertion that superoscillations stem from interference of the wavefunction with itself — similarly to the regime of single-photon superoscillations[83] — when an image of the hotspot is formed by a large number of registration single-electron events[136].

1. Atwater, H. A. The promise of plasmonics. *Sci. Am.* **296**, 56–63 (2007).
2. Brongersma, M. L. & Shalaev, V. M. The case for plasmonics. *Science* **328**, 440–441 (2010).
3. Pendry, J. B. Negative refraction makes a perfect lens. *Phys. Rev. Lett.* **85**, 3966–3969 (2000).
4. Zhang, X. & Liu, Z. W. Superlenses to overcome the diffraction limit. *Nat. Mater.* **7**, 435–441 (2008).
5. Berry, M. V. & Popescu, S. Evolution of quantum superoscillations and optical superresolution without evanescent waves. *J. Phys. A Math. Gen.* **39**, 6965–6977 (2006).
6. Berry, M. V. & Moiseyev, N. Superoscillations and supershifts in phase space: Wigner and Husimi function interpretations. *J. Phys. A Math. Theor.* **47**, 315203 (2014).
7. Wang, Q. A simple model of Aharonov-Berry's superoscillations. *J. Phys. A Math. Gen.* **29**, 2257–2258 (1996).
8. Ferreira, P., Kempf, A. & Reis, M. Construction of Aharonov–Berry's superoscillations. *J. Phys. A Math. Theor.* **40**, 5141–5147 (2007).
9. Huang, F. M. & Zheludev, N. I. Super-resolution without evanescent waves. *Nano Lett.* **9**, 1249–1254 (2009).
10. Lindberg, J. Mathematical concepts of optical superresolution. *J. Opt.* **14**, 083001 (2012).
11. Chojnacki, L. & Kempf, A. New methods for creating superoscillations. *J. Phys. A Math. Theor.* **49**, 505203 (2016).
12. Lee, D. G. & Ferreira, P. Direct construction of superoscillations. *IEEE Trans. Signal. Process.* **62**, 3125–3134 (2014).
13. Wong, A. M. H. & Eleftheriades, G. V. Adaptation of Schelkunoff's superdirective antenna theory for the realization of superoscillatory antenna arrays. *IEEE Antennas Wirel. Propag. Lett.* **9**, 315–318 (2010).
14. Chremmos, I. & Fikioris, G. Superoscillations with arbitrary polynomial shape. *J. Phys. A Math. Theor.* **48**, 265204 (2015).
15. Smith, M. K. & Gbur, G. Mathematical method for designing superresolution lenses using superoscillations. *Opt. Lett.* **45**, 1854–1857 (2020).
16. Rogers, K. S. & Rogers, E. T. F. Realising superoscillations: A review of mathematical tools and their application. *J. Phys. Photonics* **2**, 042004 (2020).
17. Zheludev, N. I. What diffraction limit? *Nat. Mater.* **7**, 420–422 (2008).
18. Karoui, A. & Moumni, T. Spectral analysis of the finite Hankel transform and circular prolate spheroidal wave functions. *J. Comput. Appl. Math.* **233**, 315–333 (2009).
19. Slepian, D. & Pollak, H. O. Prolate spheroidal wave functions, Fourier analysis and uncertainty — I. *Bell Syst. Tech. J.* **40**, 43–63 (1961).
20. Ferreira, P. & Kempf, A. Superoscillations: Faster than the Nyquist rate. *IEEE Trans. Signal. Process.* **54**, 3732–3740 (2006).
21. Kempf, A. & Ferreira, P. Unusual properties of superoscillating particles. *J. Phys. A Math. Gen.* **37**, 12067–12076 (2004).
22. Tang, E., Garg, L. & Kempf, A. Scaling properties of superoscillations and the extension to periodic signals. *J. Phys. A Math. Theor.* **49**, 335202 (2016).
23. Kempf, A. Black holes, bandwidths and Beethoven. *J. Math. Phys.* **41**, 2360–2374 (2000).
24. Shannon, C. E. A mathematical theory of communication. *Bell Syst. Tech. J.* **27**, 623–656 (1948).
25. Aharonov, Y., Albert, D. Z. & Vaidman, L. How the result of a measurement of a component of the spin of a spin-1/2 particle can turn out to be 100. *Phys. Rev. Lett.* **60**, 1351–1354 (1988).
26. Berry, M. V. & Shukla, P. Typical weak and superweak values. *J. Phys. A Math. Theor.* **43**, 354024 (2010).
27. Vigoureux, J. M., Dhooge, L. & Vanlabeke, D. Quantization of evanescent electromagnetic waves: Momentum of the electromagnetic field very close to a dielectric medium. *Phys. Rev. A* **21**, 347–355 (1980).
28. Berry, M. V. Superluminal speeds for relativistic random waves. *J. Phys. A Math. Theor.* **45**, 185308 (2012).
29. Hosten, O. & Kwiat, P. Observation of the spin Hall effect of light via weak measurements. *Science* **319**, 787–790 (2008).
30. Toraldo Di Francia, G. Super-gain antennas and optical resolving power. *Nuovo Cim.* **9**, 426–438 (1952).
31. Schelkunoff, S. A. A mathematical theory of linear arrays. *Bell Syst. Tech. J.* **22**, 80–107 (1943).
32. Leiserson, I., Lipson, S. G. & Sarafis, V. Superresolution in far-field imaging. *Opt. Lett.* **25**, 209–211 (2000).
33. Leiserson, I., Lipson, S. G. & Sarafis, V. Superresolution in far-field imaging. *J. Opt. Soc. Am. A* **19**, 436–443 (2002).
34. Huang, F. M., Zheludev, N., Chen, Y. F. & de Abajo, F. J. G. Focusing of light by a nanohole array. *Appl. Phys. Lett.* **90**, 091119 (2007).
35. Huang, F. M., Chen, Y., de Abajo, F. J. G. & Zheludev, N. I. Optical super-resolution through super-oscillations. *J. Opt. A Pure Appl. Opt.* **9**, S285–S288 (2007).
36. Rogers, K. S., Bourdakos, K. N., Yuan, G. H., Mahajan, S. & Rogers, E. T. F. Optimising superoscillatory spots for far-field super-resolution imaging. *Opt. Express* **26**, 8095–8112 (2018).
37. Maznev, A. A. & Wright, O. B. Upholding the diffraction limit in the focusing of light and sound. *Wave Motion* **68**, 182–189 (2017).
38. Padgett, M. On the focussing of light, as limited by the uncertainty principle. *J. Mod. Opt.* **55**, 3083–3089 (2008).
39. Huang, F. M., Kao, T. S., Fedotov, V. A., Chen, Y. F. & Zheludev, N. I. Nanohole array as a lens. *Nano Lett.* **8**, 2469–2472 (2008).
40. Oreopoulos, J., Berman, R. & Browne, M. in *Quantitative Imaging in Cell Biology* Vol. 123 (eds Waters, J. C. & Wittmann, T.) 153–175 (Academic, 2014).
41. Wang, Q. et al. Reconfigurable phase-change photomask for grayscale photolithography. *Appl. Phys. Lett.* **110**, 201110 (2017).
42. Lee, W. H. Binary computer-generated holograms. *Appl. Opt.* **18**, 3661–3669 (1979).
43. Rogers, E. T. F. et al. A super-oscillatory lens optical microscope for subwavelength imaging. *Nat. Mater.* **11**, 432–435 (2012).
44. Chen, G. et al. Generation of a sub-diffraction hollow ring by shaping an azimuthally polarized wave. *Sci. Rep.* **6**, 37776 (2016).
45. Wu, Z. X. et al. Generating a three-dimensional hollow spot with sub-diffraction transverse size by a focused cylindrical vector wave. *Opt. Express* **26**, 7866–7875 (2018).
46. Qin, F. et al. A supercritical lens optical label-free microscopy: sub-diffraction resolution and ultra-long working distance. *Adv. Mater.* **29**, 1602721 (2017).
47. Zhu, X. F. et al. Supercritical lens array in a centimeter scale patterned with maskless UV lithography. *Opt. Lett.* **45**, 1798–1801 (2020).
48. Chen, G., Wen, Z. Q. & Qiu, C. W. Superoscillation: from physics to optical applications. *Light Sci. Appl.* **8**, 56 (2019).
49. Legaria, S., Pacheco-Pena, V. & Beruete, M. Super-oscillatory metalens at terahertz for enhanced focusing with reduced side lobes. *Photonics* **5**, 56 (2018).
50. Liu, T., Shen, T., Yang, S. M. & Jiang, Z. D. Subwavelength focusing by binary multi-annularplates: design theory and experiment. *J. Opt.* **17**, 035610 (2015).
51. Chen, G. et al. Far-field sub-diffraction focusing lens based on binary amplitude-phase mask for linearly polarized light. *Opt. Express* **24**, 11002–11008 (2016).
52. Chen, G. et al. Super-oscillatory focusing of circularly polarized light by ultra-long focal length planar lens based on binary amplitude-phase modulation. *Sci. Rep.* **6**, 29068 (2016).
53. Li, M. Y., Li, W. L., Li, H. Y., Zhu, Y. C. & Yu, Y. T. Controllable design of super-oscillatory lenses with multiple sub-diffraction-limit foci. *Sci. Rep.* **7**, 1335 (2017).
54. Huang, K. et al. Optimization-free superoscillatory lens using phase and amplitude masks. *Laser Photonics Rev.* **8**, 152–157 (2014).
55. Wu, Z. X. et al. Optimization-free approach for generating sub-diffraction quasi-non-diffracting beams. *Opt. Express* **26**, 16585–16599 (2018).
56. Rogers, E. T. F. & Zheludev, N. I. Optical super-oscillations: sub-wavelength light focusing and super-resolution imaging. *J. Opt.* **15**, 094008 (2013).
57. Huang, K. et al. Ultrahigh-capacity non-periodic photon sieves operating in visible light. *Nat. Commun.* **6**, 7059 (2015).
58. Qin, F. et al. Shaping a subwavelength needle with ultra-long focal length by focusing azimuthally polarized light. *Sci. Rep.* **5**, 09977 (2015).
59. Yu, Y. T., Li, W. L., Li, H. Y., Li, M. Y. & Yuan, W. Z. An investigation of influencing factors on practical sub-diffraction-limit focusing of planar super-oscillation lenses. *Nanomaterials* **8**, 185 (2018).
60. Yuan, G. H., Rogers, E. T. F. & Zheludev, N. I. Achromatic super-oscillatory lenses with sub-wavelength focusing. *Light Sci. Appl.* **6**, e17036 (2017).
61. Wang, Z. et al. Exciton-enabled meta-optics in two-dimensional transition metal dichalcogenides. *Nano Lett.* **20**, 7964–7972 (2020).
62. Yuan, G. H., Lin, Y. H., Tsai, D. P. & Zheludev, N. I. Superoscillatory quartz lens with effective numerical aperture greater than one. *Appl. Phys. Lett.* **117**, 021106 (2020).
63. Li, W. L., Yu, Y. T. & Yuan, W. Z. Flexible focusing pattern realization of centimeter-scale planar super-oscillatory lenses in parallel fabrication. *Nanoscale* **11**, 311–320 (2019).
64. Wang, Q. et al. Optically reconfigurable metasurfaces and photonic devices based on phase change materials. *Nat. Photonics* **10**, 60–65 (2016).
65. Yu, N. F. & Capasso, F. Flat optics with designer metasurfaces. *Nat. Mater.* **13**, 139–150 (2014).
66. Khorasaninejad, M. et al. Metalenses at visible wavelengths: Diffraction-limited focusing and subwavelength resolution imaging. *Science* **352**, 1190–1194 (2016).
67. Roy, T., Yuan, G. H., Rogers, E. T. F. & Zheludev, N. I. in *2014 Conference on Lasers and Electro-Optics (CLEO)* FW3K.3 (IEEE, 2014).
68. Yuan, G. H., Rogers, E. T. F., Roy, T., Shen, Z. X. & Zheludev, N. I. Flat super-oscillatory lens for heat-assisted magnetic recording with sub-50nm resolution. *Opt. Express* **22**, 6428–6437 (2014).
69. Banerji, S., Meem, M., Majumder, A., Sensale-Rodriguez, B. & Menon, R. Extreme-depth-of-focus imaging with a flat lens. *Optica* **7**, 214–217 (2020).
70. Oseen, C. W. Einstein's pinprick radiation and Maxwell's equations. *Ann. Phys.* **69**, 202–204 (1922).
71. Rogers, E. T. F. et al. Super-oscillatory optical needle. *Appl. Phys. Lett.* **102**, 031108 (2013).
72. Roy, T., Rogers, E. T. F., Yuan, G. H. & Zheludev, N. I. Point spread function of the optical needle super-oscillatory lens. *Appl. Phys. Lett.* **104**, 231109 (2014).
73. Yuan, G. H. et al. Planar super-oscillatory lens for sub-diffraction optical needles at violet wavelengths. *Sci. Rep.* **4**, 6333 (2014).
74. Diao, J. S., Yuan, W. Z., Yu, Y. T., Zhu, Y. C. & Wu, Y. Controllable design of super-oscillatory planar lenses for sub-diffraction-limit optical needles. *Opt. Express* **24**, 1924–1933 (2016).
75. Chen, G. et al. Planar binary-phase lens for super-oscillatory optical hollow needles. *Sci. Rep.* **7**, 4697 (2017).
76. Kryder, M. H. et al. Heat assisted magnetic recording. *Proc. IEEE* **96**, 1810–1835 (2008).
77. Yuan, G. H. et al. in *2013 Conference on Lasers and Electro-Optics (CLEO)* QM1B.8 (IEEE, 2013).
78. Yuan, G. H., Rogers, K. S., Rogers, E. T. F. & Zheludev, N. I. Far-field superoscillatory metamaterial superlens. *Phys. Rev. Appl.* **11**, 064016 (2019).
79. Papakostas, A. et al. Optical manifestations of planar chirality. *Phys. Rev. Lett.* **90**, 107404 (2003).
80. Yu, N. F. et al. Light propagation with phase discontinuities: generalized laws of reflection and refraction. *Science* **334**, 333–337 (2011).
81. Tang, D. L. et al. Ultrabroadband superoscillatory lens composed by plasmonic metasurfaces for subdiffraction light focusing. *Laser Photonics Rev.* **9**, 713–719 (2015).
82. Li, Z. et al. Achromatic broadband super-resolution imaging by super-oscillatory metasurface. *Laser Photonics Rev.* **12**, 180064 (2018).
83. Yuan, G. H. et al. Quantum super-oscillation of a single photon. *Light Sci. Appl.* **5**, e16127 (2016).
84. Rueckner, W. & Peidle, J. Young's double-slit experiment with single photons and quantum eraser. *Am. J. Phys.* **81**, 951–958 (2013).
85. Huignard, J. P. Spatial light modulators and their applications. *J. Opt.* **18**, 181–186 (1987).
86. Maurer, C., Jesacher, A., Bernet, S. & Ritsch-Marte, M. What spatial light modulators can do for optical microscopy. *Laser Photonics Rev.* **5**, 81–101 (2011).
87. Rogers, E. T. F. et al. Far-field unlabeled super-resolution imaging with superoscillatory illumination. *APL Photonics* **5**, 066107 (2020).
88. Singh, B. K., Nagar, H., Roichman, Y. & Arie, A. Particle manipulation beyond the diffraction limit using structured super-oscillating light beams. *Light Sci. Appl.* **6**, e17050 (2017).

89. Singh, B. K., Nagar, H., Roichman, Y. & Arie, A. in *Optical Trapping and Optical Micromanipulation XV* Vol. 10723 (eds Dholakia, K. & Spalding, G. C.) 1072303 (SPIE, 2018).
90. Johnson, C. W. et al. Exact design of complex amplitude holograms for producing arbitrary scalar fields. *Opt. Express* **28**, 17334–17346 (2020).
91. Wan, Z. S., Wang, Z. Y., Yang, X. L., Shen, Y. J. & Fu, X. Digitally tailoring arbitrary structured light of generalized ray-wave duality. *Opt. Express* **28**, 31043–31056 (2020).
92. Zacharias, T. & Bahabad, A. Light beams with volume superoscillations. *Opt. Lett.* **45**, 3482–3485 (2020).
93. Woodward, B. P. M. The theoretical precision with which an arbitrary radiation-pattern may be obtained from a source of finite size. *J. Inst. Electr. Eng.* **95**, 363–370 (1948).
94. Bouwkamp, C. J. & De Bruin, N. G. The problem of optimum antenna current distribution. *Phillips Res. Rep.* **1**, 135–158 (1945).
95. Ruan, D. S. et al. Realizing a terahertz far-field sub-diffraction optical needle with sub-wavelength concentric ring structure array. *Appl. Opt.* **57**, 7905–7909 (2018).
96. Yang, M. Y. et al. Subdiffraction focusing of total electric fields of terahertz wave. *Opt. Commun.* **458**, 124764 (2020).
97. Shen, Y. X. et al. Ultrasonic super-oscillation wave-packets with an acoustic meta-lens. *Nat. Commun.* **10**, 3411 (2019).
98. Hyun, J. et al. Realization of an ultrathin acoustic lens for subwavelength focusing in the megasonic range. *Sci. Rep.* **8**, 9131 (2018).
99. Wong, A. M. H. & Eleftheriades, G. V. Sub-wavelength focusing at the multi-wavelength range using superoscillations: an experimental demonstration. *IEEE Trans. Antennas Propag.* **59**, 4766–4776 (2011).
100. Wong, A. M. H. & Eleftheriades, G. V. Superoscillatory radar imaging: improving radar range resolution beyond fundamental bandwidth limitations. *IEEE Microw. Wirel. Compon. Lett.* **22**, 147–149 (2012).
101. Berry, M. V. & Dennis, M. R. Natural superoscillations in monochromatic waves in D dimensions. *J. Phys. A Math. Theor.* **42**, 022003 (2009).
102. Dennis, M. R., Hamilton, A. C. & Courtial, J. Superoscillation in speckle patterns. *Opt. Lett.* **33**, 2976–2978 (2008).
103. Berry, M. V. Quantum backflow, negative kinetic energy, and optical retro-propagation. *J. Phys. A Math. Theor.* **43**, 415302 (2010).
104. Eliezer, Y., Zacharias, T. & Bahabad, A. Observation of optical backflow. *Optica* **7**, 72–76 (2020).
105. Yuan, G. H., Rogers, E. T. F. & Zheludev, N. I. "Plasmonics" in free space: observation of giant wavevectors, vortices, and energy backflow in superoscillatory optical fields. *Light Sci. Appl.* **8**, 2 (2019).
106. Bashevoy, M. V., Fedotov, V. A. & Zheludev, N. I. Optical whirlpool on an absorbing metallic nanoparticle. *Opt. Express* **13**, 8372–8379 (2005).
107. Yuan, G. H. & Zheludev, N. I. Detecting nanometric displacements with optical ruler metrology. *Science* **364**, 771–775 (2019).
108. Nye, J. F., Berry, M. V. & Walford, M. E. R. Measuring the change in thickness of the Antarctic ice sheet. *Nat. Phys. Sci.* **240**, 7–9 (1972).
109. Betzig, E. et al. Imaging intracellular fluorescent proteins at nanometer resolution. *Science* **313**, 1642–1645 (2006).
110. Blom, H. & Widengren, J. Stimulated emission depletion microscopy. *Chem. Rev.* **117**, 7377–7427 (2017).
111. Wang, C. T. et al. Super-resolution optical telescopes with local light diffraction shrinkage. *Sci. Rep.* **5**, 18485 (2015).
112. Rogers, E. T. F. et al. New super-oscillatory technology for unlabelled super-resolution cellular imaging with polarisation contrast. *Biophys. J.* **112**, 186a (2017).
113. Shapira, N. et al. Multi-lobe superoscillation and its application to structured illumination microscopy. *Opt. Express* **27**, 34530–34541 (2019).
114. Wong, A. M. H. & Eleftheriades, G. V. An optical super-microscope for far-field, real-time imaging beyond the diffraction limit. *Sci. Rep.* **3**, 1715 (2013).
115. Thibault, P. & Elser, V. X-ray diffraction microscopy. *Annu. Rev. Condens. Matter Phys.* **1**, 237–255 (2010).
116. Gazit, S., Szameit, A., Eldar, Y. C. & Segev, M. Super-resolution and reconstruction of sparse sub-wavelength images. *Opt. Express* **17**, 23920–23946 (2009).
117. Vemuri, V. & Jang, G. S. Inversion of Fredholm integral equations of the first kind with fully connected neural networks. *J. Frankl. Inst. Eng. Appl. Math.* **329**, 241–257 (1992).
118. Rivenson, Y. et al. Deep learning microscopy. *Optica* **4**, 1437–1443 (2017).
119. Ouyang, W., Aristov, A., Lelek, M., Hao, X. & Zimmer, C. Deep learning massively accelerates super-resolution localization microscopy. *Nat. Biotechnol.* **36**, 460–468 (2018).
120. Wang, H. D. et al. Deep learning enables cross-modality super-resolution in fluorescence microscopy. *Nat. Methods* **16**, 103–110 (2019).
121. Piccinotti, D., MacDonald, K. F., Gregory, S., Youngs, I. & Zheludev, N. I. Artificial intelligence for photonics and photonic materials. *Rep. Prog. Phys.* **84**, 012401 (2020).
122. Pu, T., Ou, J. Y., Papasimakis, N. & Zheludev, N. I. Label-free deeply subwavelength optical microscopy. *Appl. Phys. Lett.* **116**, 131105 (2020).
123. Rendon-Barraza, C. et al. Deeply sub-wavelength non-contact optical metrology of sub-wavelength objects. *APL Photonics* **6**, 066107 (2021).
124. Chan, E. A. et al. in *Conference on Lasers and Electro-Optics/Europe — European Quantum Electronics Virtual Conferences* (CLEO, 2021).
125. Pu, T. et al. Unlabeled far-field deeply subwavelength topological microscopy (DSTM). *Adv. Sci.* **2020**, 2002886 (2020).
126. Narimanov, E. Resolution limit of label-free far-field microscopy. *Adv. Photonics* **1**, 056003 (2019).
127. Huang, K. et al. Planar diffractive lenses: fundamentals, functionalities, and applications. *Adv. Mater.* **30**, 1704556 (2018).
128. Berry, M. et al. Roadmap on superoscillations. *J. Opt.* **21**, 053002 (2019).
129. Gbur, G. Using superoscillations for superresolved imaging and subwavelength focusing. *Nanophotonics* **8**, 205–225 (2019).
130. Eliezer, Y., Hareli, L., Lobachinsky, L., Froim, S. & Bahabad, A. Breaking the temporal resolution limit by superoscillating optical beats. *Phys. Rev. Lett.* **119**, 043903 (2017).
131. Wong, A. M. H. & Eleftheriades, G. V. Temporal pulse compression beyond the Fourier transform limit. *IEEE Trans. Microw. Theory Tech.* **59**, 2173–2179 (2011).
132. Eliezer, Y. & Bahabad, A. Super-transmission: the delivery of superoscillations through the absorbing resonance of a dielectric medium. *Opt. Express* **22**, 31212–31226 (2014).
133. Zarkovsky, S., Ben-Ezra, Y. & Schwartz, M. Transmission of superoscillations. *Sci. Rep.* **10**, 5893 (2020).
134. Remez, R. & Arie, A. Super-narrow frequency conversion. *Optica* **2**, 472–475 (2015).
135. Eliezer, Y. & Bahabad, A. Super defocusing of light by optical sub-oscillations. *Optica* **4**, 440–446 (2017).
136. Remez, R. et al. Superoscillating electron wave functions with subdiffraction spots. *Phys. Rev. A* **95**, 031802(R) (2017).
137. Piccinotti, D. et al. Optical response of nanohole arrays filled with chalcogenide low-epsilon media. *Adv. Opt. Mater.* **6**, 1800395 (2018).

Author contributions
The authors made equal contributions to the paper.

Competing interests
The authors declare no competing interests.

Peer review information
Nature Reviews Physics thanks A. Bahabad, G. Gbur and the other, anonymous, reviewer(s) for their contribution to the peer review of this work.

Publisher's note
Springer Nature remains neutral with regard to jurisdictional claims in published maps and institutional affiliations.

Supplementary information
The online version contains supplementary material available at https://doi.org/10.1038/s42254-021-00382-7.